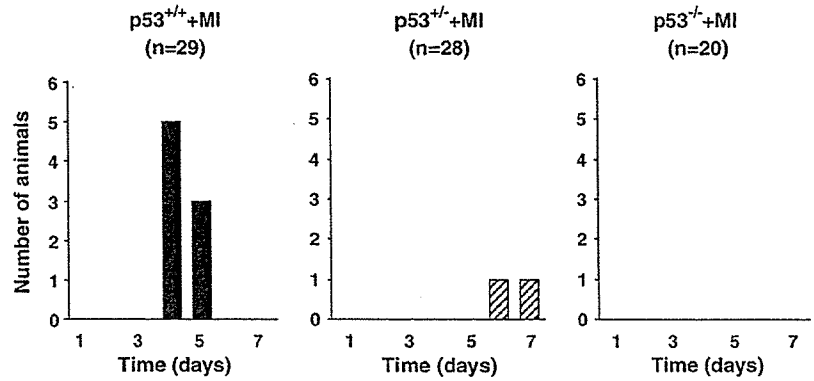

Fig. 3. The number of animals died of cardiac rupture in the $p53^{+/+}$+MI, $p53^{+/-}$+MI, and $p53^{-/-}$+MI mice.

antibody against phospho (Ser473)-Akt and Akt (Cell Signaling). In brief, the LV tissue was homogenized with the lysis buffer (25 mmol/L Tris, 150 mmol/L NaCl, 5 mmol/L EDTA, 1 mmol/L Na_3VO_4; pH 7.4). After centrifugation, equal amounts of protein (15 μg protein/lane), estimated by the Bradford method using a protein assay (Bio-Rad), were electrophoresed on a 12.5% SDS-polyacrylamide gel, and then electrophoretically transferred to a nitrocellulose membrane (Millipore). After blocking with 2.5% nonfat milk in TBS containing 0.1% Tween 20 at room temperature for 30 min, the membrane was incubated with the first antibody, and then with the peroxidase-linked second antibody (Santa Cruz). Chemiluminescence was detected with an ECL Western blot detection kit (Amersham Pharmacia) according to the manufacturer's recommendation.

2.5. Statistical analysis

All data are expressed as the means±S.E.M. A survival analysis was performed by the Kaplan–Meier method, and between-group difference in survival was tested by the logrank test. Between-group comparisons of the means were performed by one-way ANOVA, followed by *t*-tests. The Bonferroni's correction was done for multiple comparisons of the means.

3. Results

3.1. Experimental protocol 1: 7-day post-MI study

3.1.1. Survival and LV rupture

$p53^{+/-}$+MI and $p53^{-/-}$+MI mice had significantly better survival than $p53^{+/+}$+MI mice (Fig. 2). The number of the mice that died of LV rupture was significantly less in $p53^{-/-}$+MI and $p53^{+/-}$+MI than in $p53^{+/+}$+MI mice (Fig. 3). There were no deaths in the sham-operated groups. There were no significant differences in the survival rate among these 3 groups of survivor mice followed after 7 days up to 4 weeks.

3.2. Experimental protocol 2: 3-day post-MI study

3.2.1. Echocardiography and hemodynamics

The echocardiographic and hemodynamic data of the surviving mice at 3 days of MI are shown in Table 1. The LV diameters increased and fractional shortening decreased significantly in the $p53^{+/+}$+MI, $p53^{+/-}$+MI, and $p53^{-/-}$+

Table 1
Echocardiographic and hemodynamic data at 3 days after surgery

	$p53^{+/+}$+Sham	$p53^{+/-}$+Sham	$p53^{+/+}$+MI	$p53^{+/-}$+MI	$p53^{-/-}$+MI
Echocardiographic data					
n	7	7	13	12	7
Heart rate, bpm	491±3	487±5	492±7	493±5	484±15
LVEDD, mm	3.7±0.1	3.7±0.1	4.6±0.1**	4.7±0.1**	4.7±0.1**
LVESD, mm	2.3±0.0	2.3±0.1	3.9±0.1**	3.8±0.1**	3.8±0.1**
Fractional shortening, %	36.6±0.4	37.7±0.4	16.5±1.0**	17.9±0.7**	19.2±1.0**
Hemodynamic data					
n	7	7	11	10	5
Heart rate, bpm	492±14	491±10	481±15	490±13	494±6
Mean aortic pressure, mm Hg	79±4	79±2	77±2	79±2	74±1
LVEDP, mm Hg	1.3±0.4	1.3±0.4	12.0±1.9**	11.7±2.9**	10.2±2.8**
LV dP/dt_{max}, mm Hg/s	9055±1133	8299±332	5927±409**	5710±240**	6417±466**

MI, myocardial infarction. LV, left ventricular. EDD, end-diastolic diameter. ESD, end-systolic diameter. EDP, end-diastolic pressure. bpm, beats per min. Values are means±S.E.M. **$P<0.01$ vs. $p53^{+/-}$+Sham.

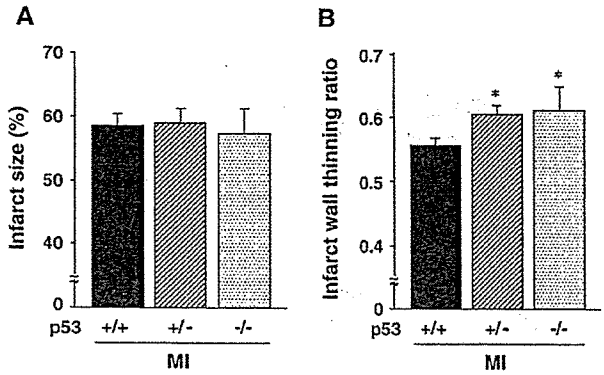

Fig. 4. Infarct size (A) and infarct wall thinning ratio (B) in $p53^{+/+}$-MI, $p53^{+/-}$MI, and $p53^{-/-}$MI mice ($n=6$ each). Values are means±S.E.M. *$P<0.05$ for difference from the $p53^{+/+}$+MI.

MI mice compared to sham operated mice. However, these changes were comparable among $p53^{+/+}$+MI, $p53^{+/-}$+MI, and $p53^{-/-}$+MI.

There was no significant difference in the heart rate and mean aortic blood pressure among 5 groups of mice. The LV end-diastolic pressure (EDP) increased and LV dP/dt_{max} decreased in $p53^{+/+}$+MI compared to sham, which was similarly observed in $p53^{+/-}$+MI and $p53^{-/-}$+MI.

3.2.2. Infarct size and wall thickness

The infarct size determined by the morphometric analysis at 3 days of MI was comparable among the $p53^{+/+}$+MI, $p53^{+/-}$+MI, and $p53^{-/-}$+MI ($n=6$ each) mice (Fig. 4A). Moreover, percentages of LV at risk (risk area/LV; 60.4±5.2% vs. 59.1±2.8%, P=NS) and the infarct size (infarct/risk area; 58.7±7.8% vs. 61.4±2.5%, P=NS) measured by Evans blue and TTC staining at 24 h of MI were also comparable between $p53^{+/-}$+MI and $p53^{+/+}$+MI ($n=5$ each).

The thickness of the infarcted LV wall and that of the noninfarcted LV in $p53^{-/-}$+MI were 0.43±0.02 and 0.70±0.03 mm, respectively, those in $p53^{+/-}$+MI were 0.41±0.02 and 0.67±0.03 mm, respectively, and those in $p53^{+/+}$+MI were 0.39±0.01 and 0.70±0.02 mm, respectively. Thus infarct wall thinning ratio, the thickness of the infarcted LV wall normalized to that of the noninfarcted LV, was significantly greater in $p53^{-/-}$+MI or $p53^{+/-}$+MI than in $p53^{+/+}$+MI (Fig. 4B).

3.2.3. Myocardial histopathology

MI mice had more infiltrating interstitial cells in the border zone and infarcted myocardium than sham-operated mice. However, the extent of infiltration was comparable among $p53^{+/+}$+MI, $p53^{+/-}$+MI, and $p53^{-/-}$+MI (Fig. 5A). Moreover, the infiltration of macrophages was similar between groups (Fig. 5B).

Interstitial fibrosis, measured as collagen volume fraction, in the infarcted as well as border zone LV was also comparable among $p53^{+/+}$+MI, $p53^{+/-}$+MI, and $p53^{-/-}$+MI (Fig. 6A).

3.2.4. MMPs

The zymographic MMP-2 and MMP-9 levels significantly increased in the infarcted LV from MI groups, however, no difference in this regard was seen between $p53^{+/+}$+MI and $p53^{+/-}$+MI mice (Fig. 6B).

3.2.5. Myocardial apoptosis

There were rare TUNEL-positive nuclei in sham-operated mice. The number of TUNEL-positive cells was increased in $p53^{+/+}$+MI, which was significantly prevented in $p53^{+/-}$+MI and $p53^{-/-}$+MI (Fig. 7A). In addition, DNA ladder appeared faint in the infarcted LV from $p53^{+/-}$+MI compared to that from $p53^{+/+}$+MI (Fig. 7B).

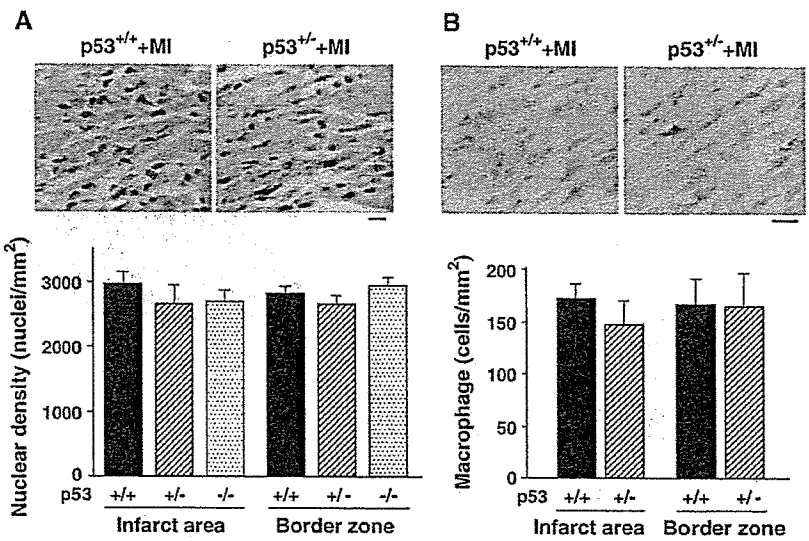

Fig. 5. Representative photomicrographs of LV sections and summary data for nuclear density of infiltrating cells stained with hematoxylin and eosin (A) and macrophages (B) at the infarct area and border zone. Scale bar, 10 μm. Values are means±S.E.M. ($n=6$ each).

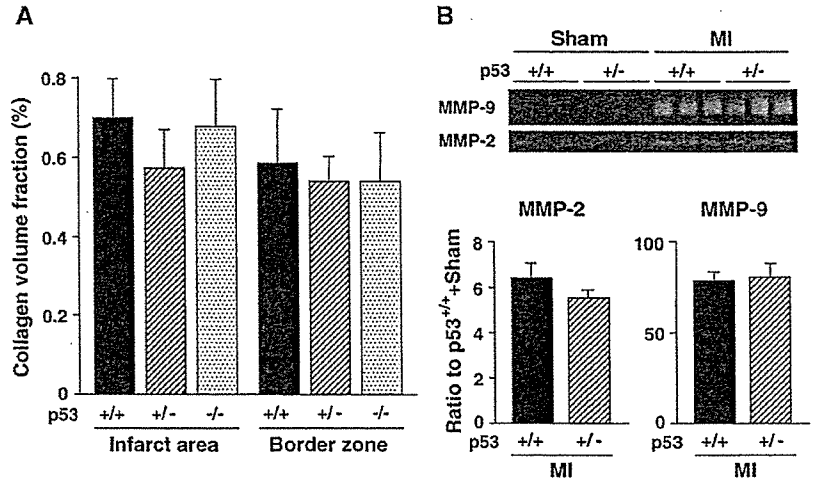

Fig. 6. (A) Summary data of collagen volume fraction at the infarcted area and border zone of LV tissue sections ($n=6$ for each). (B) Representative LV zymographic MMP-2 and MMP-9 levels and summary data at 3 days of MI ($n=6$ for each).

3.2.6. Akt protein

Either Akt protein (total) or phospho-Akt levels did not differ between 4 groups of $p53^{+/+}$+Sham, $p53^{+/-}$+Sham, $p53^{+/+}$+MI, and $p53^{+/-}$+MI mice (Fig. 8).

4. Discussion

The major new finding of the present study is the significant improvement in the survival of MI mice by the targeted deletion of p53 gene, which was mainly attributable to the inhibition of early LV rupture. After MI, p53-dependent apoptosis might contribute to the thinning of the infarct wall and eventual LV rupture. Our observations thus suggest that an anti-p53 strategy may be of therapeutic benefit against the evolution of cardiac rupture after MI.

Cardiac rupture is the most drastic and severe complication of acute MI. Following MI, a reparative process, infarct healing, is immediately initiated, including inflammatory cell infiltration, activation of MMPs, extracellular matrix remodeling and scar formation. Thinning of the infarcted wall and dilatation of LV cavity, which occur during the acute phase of MI, are termed as "infarct expansion" [1]. The delay or impairment of this process may jeopardize infarct healing, aggravate extracellular matrix remodeling, and cause cardiac rupture. Previous studies demonstrated that p53 was increased [8] and apoptosis of cardiac myocytes were detected in the infarcted regions during the

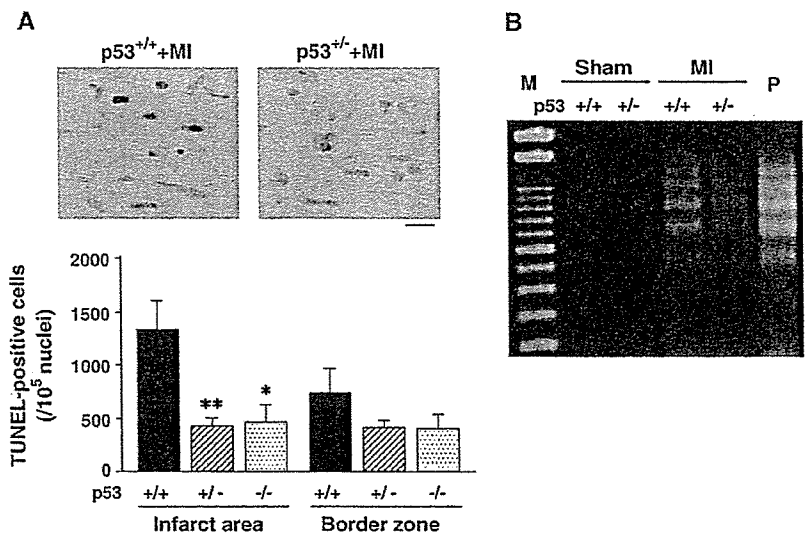

Fig. 7. (A) Representative photomicrographs of LV sections and summary data for the number of TUNEL-positive cells in the infarcted area and border zone of LV ($n=6$ each). Scale bar, 10 μm. Values are means±S.E.M. *$P<0.05$, **$P<0.01$ for difference from the $p53^{+/+}$+MI values. (B) DNA ladder indicative of apoptosis in the genomic DNA from the LV. M, marker. P, positive control.

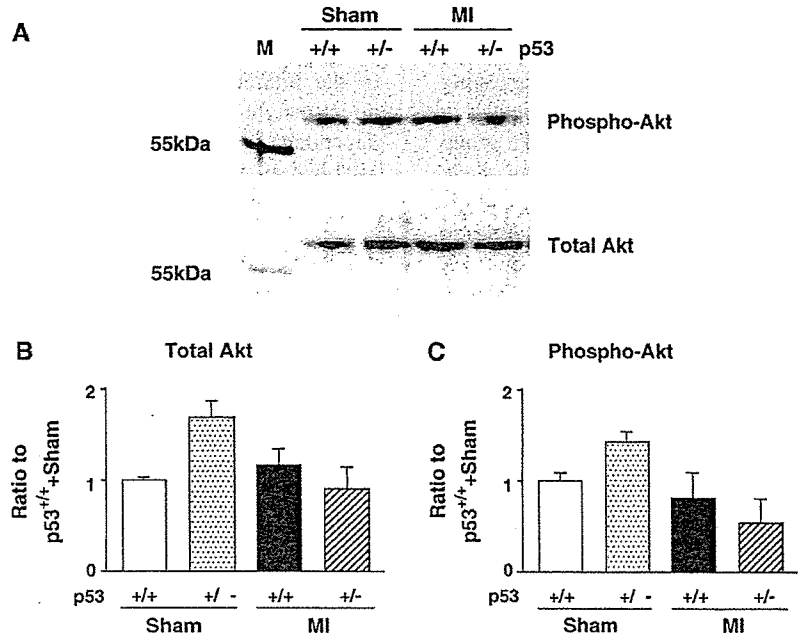

Fig. 8. (A) Representative Western blot analysis of Akt (total) and phospho-Akt protein levels in LV tissue obtained from 4 groups of $p53^{+/+}$+Sham, $p53^{+/-}$+Sham, $p53^{+/+}$+MI, and $p53^{+/-}$+MI mice. Summary data for total Akt (B) and phospho-Akt (C) protein levels in $p53^{+/+}$+Sham, $p53^{+/-}$+Sham, $p53^{+/+}$+MI, and $p53^{+/-}$+MI mice ($n=3$ for each). M, marker.

early days after MI [9,10]. Therefore, p53-dependent apoptosis at the infarcted myocardium may contribute to cardiac rupture. However, no previous studies have provided direct evidence supporting this notion. The present study has demonstrated that p53 is indeed involved in cardiac rupture after MI (Fig. 3) via mediating apoptosis (Fig. 7) and wall thinning at the infarct area (Fig. 4B).

The beneficial effects of p53 deletion were not due to its MI size-sparing effects because the infarct size was comparable between the $p53^{+/+}$ and $p53^{+/-}$ mice (Fig. 4A). Further, its effects might not be attributable to those on hemodynamics because the blood pressure and heart rate showed no alterations (Table 1). In addition, inflammatory cell infiltration and inadequate fibrosis have been postulated to cause myocyte separation in the infarct area, which may lead to eventual cardiac rupture [4]. However, the present study could not find any alterations in the infiltration of inflammatory cells or collagen deposition between $p53^{+/+}$ and $p53^{+/-}$ mice after MI (Figs. 5 and 6A). Further, even though recent studies have demonstrated that the inhibition of MMPs can prevent cardiac rupture [4,5], targeted deletion of p53 gene did not affect the increase in MMP-2 or MMP-9 activities in the post-MI hearts in the present study (Fig. 6B). These lines of evidence indicate that the inhibition of cardiac rupture in $p53^{+/-}$ mice was not due to the altered reparative process of extracellular matrix or the infiltration of inflammatory cells and further confirm the significance of attenuated apoptosis and infarct wall thinning in the prevention of cardiac rupture.

Previous experimental [9] and human [10] studies have detected TUNEL-positive cells in the post-MI hearts. Even though they implicated apoptosis in the pathogenesis of late LV remodeling after MI [19], it may also contribute to the early phase structural alterations known to occur within the infarct area, which is characterized by a significant net loss of cardiac myocytes as well as myocyte slippage and elongation [24]. However, the significance of myocardial apoptosis in this phase of MI has been mostly speculative. Thus the present study clearly demonstrated for the first time that p53-dependent apoptosis is involved not only in late remodeling after MI [19] but also in early cardiac rupture.

The present study was in contrast to the previous study by Bialik et al., in which myocyte apoptosis was not altered after MI in the hearts of mice nullizygous for p53 [25]. It is difficult, however, to find identical experimental conditions between their study and the present study by that would be necessary for a direct comparison; the age of the animals (6–8 weeks in the study by Bialik vs. 10–14 weeks in this study) and the time at which apoptosis was assessed (10 and 48 h vs. 3 days). In addition, the infarct size was comparable between $p53^{-/-}$ and $p53^{+/-}$ in the present study although it was not clearly mentioned in the study by Bialik. Although the present study demonstrated the survival benefit in p53 deletion, no survival data were provided in their study.

p53 is known to be dynamically regulated via Akt, a serine/threonine kinase, that promotes cell survival [26]. Specifically, proapoptotic stimulation leads to p53-dependent destruction of Akt whereas Akt activation leads to inhibition of p53. The state of this signaling network determines the fate of the cell to survive or to enter apoptosis or hypertrophy. However, either Akt protein

(total) or phospho-Akt levels did not differ between 4 groups of $p53^{+/+}$+Sham, $p53^{+/-}$+Sham, $p53^{+/+}$+MI, and $p53^{+/-}$+MI mice in the present study (Fig. 8), suggesting that Akt might not play a major role in myocyte apoptosis in this model. Moreover, a recent study by Dr. Field's group has demonstrated that p193 and p53 exert a cell cycle regulatory role in the adult heart [27]. In their studies, target expression of the p193 and/or the p53 dominant-interfering mutants increased cardiac myocyte DNA synthesis after MI in mice, suggesting that cardiac cell cycle reentry is regulated by these proapoptotic proteins. Therefore, we could not exclude the possibility that p193 might also be involved in post-MI remodeling.

Even though the previous studies reported a difference in the phenotype between $p53^{-/-}$ and $p53^{+/-}$ mice [15,16], the echocardiographic data (Table 1), hemodynamic data (Table 1), infarct size (Fig. 4), infarct wall thinning ratio (Fig. 4), nuclear density (Fig. 5), collagen volume fraction by myocardial histopathology (Fig. 6), and the number of TUNEL-positive cells (Fig. 7) were comparable between these 2 groups of mice in the present study. Based on these results, there might be a threshold in the effects of p53 gene expression on cardiac pathophysiology after MI.

There are several limitations to be acknowledged in this study. First, although p53 is activated in the post-MI hearts [8], the mechanisms responsible for this activation are not determined in the present study. One important aspect of ischemia is prolonged hypoxia, which has been shown to increase p53 expression and result in apoptosis in cultured cardiac myocytes [6]. Furthermore, oxidative stress, which is also increased in post-MI hearts, is a powerful inducer of apoptosis [28]. However, further studies are needed to clarify the mechanisms for the modulation of p53 after MI. Second, even though the previous study demonstrated that p53 expression was increased in post-MI rat hearts [8], the present study did not determine whether endogenous p53 expression was altered in post-MI mouse hearts. Third, p53-dependent apoptotic pathways may not be a sole mechanism for cardiac rupture after MI. Cardiac repair after MI is a highly complex process, involving diverse inflammatory and growth factor signaling pathways, and extracellular matrix remodeling. Thus the mechanisms other than p53 may be also involved in this deleterious complication. Fourth, echocardiographic assessment of LV function in mice is known to be difficult. However, intra- and interobserver variabilities of our echocardiographic measurements for LV cavity dimensions and fractional shortening were small and measurements were highly reproducible [14]. Therefore, our technique was capable of noninvasively assessing the LV structure and function in mice with a large MI.

Cardiac rupture usually occurs unexpectedly and is often fatal, thereby resulting in one of the major causes of in-hospital death in patients with acute MI. It is difficult to predict its occurrence by the previously reported clinical risk factors such as aging, hypertension, and delayed thrombolysis [29]. We found that target deletion of p53 had a significantly reduced cardiac rupture rate after MI. This was accompanied by a reduction of apoptosis and wall thinning of the infarcted myocardium. Our results may provide a novel insight regarding the pathophysiological role of p53-dependent apoptosis in cardiac rupture and thus help to establish an effective therapeutic strategy.

Acknowledgments

This study was supported in part by grants from the Ministry of Education, Science and Culture (Nos. 120670676, 14370230, 17390223). A part of this study was conducted in Kyushu University Station for Collaborative Research I and II.

References

[1] Pfeffer JM, Pfeffer MA, Fletcher PJ, Braunwald E. Progressive ventricular remodeling in rat with myocardial infarction. Am J Physiol 1991;260:H1406–14.
[2] Anzai T, Yoshikawa T, Shiraki H, Asakura Y, Akaishi M, Mitamura H, et al. C-reactive protein as a predictor of infarct expansion and cardiac rupture after a first Q-wave acute myocardial infarction. Circulation 1997;96:778–84.
[3] Przyklenk K, Connelly CM, McLaughlin RJ, Kloner RA, Apstein CS. Effect of myocyte necrosis on strength, strain, and stiffness of isolated myocardial strips. Am Heart J 1987;114:1349–59.
[4] Heymans S, Luttun A, Nuyens D, Theilmeier G, Creemers E, Moons L, et al. Inhibition of plasminogen activators or matrix metalloproteinases prevents cardiac rupture but impairs therapeutic angiogenesis and causes cardiac failure. Nat Med 1999;5:1135–42.
[5] Matsumura S, Iwanaga S, Mochizuki S, Okamoto H, Ogawa S, Okada Y. Targeted deletion or pharmacological inhibition of MMP-2 prevents cardiac rupture after myocardial infarction in mice. J Clin Invest 2005;115:599–609.
[6] Long X, Boluyt MO, Hipolito ML, Lundberg MS, Zheng JS, O'Neill L, et al. p53 and the hypoxia-induced apoptosis of cultured neonatal rat cardiac myocytes. J Clin Invest 1997;99:2635–43.
[7] Polyak K, Xia Y, Zweier JL, Kinzler KW, Vogelstein B. A model for p53-induced apoptosis. Nature 1997;389:300–5.
[8] Oskarsson HJ, Coppey L, Weiss RM, Li WG. Antioxidants attenuate myocyte apoptosis in the remote non-infarcted myocardium following large myocardial infarction. Cardiovasc Res 2000;45:679–87.
[9] Kajstura J, Cheng W, Reiss K, Clark WA, Sonnenblick EH, Krajewski S, et al. Apoptotic and necrotic myocyte cell deaths are independent contributing variables of infarct size in rats. Lab Invest 1996;74:86–107.
[10] Saraste A, Pulkki K, Kallajoki M, Henriksen K, Parvinen M, Voipio-Pulkki LM. Apoptosis in human acute myocardial infarction. Circulation 1997;95:320–3.
[11] Mayr U, Mayr M, Li C, Wernig F, Dietrich H, Hu Y, et al. Loss of p53 accelerates neointimal lesions of vein bypass grafts in mice. Circ Res 2002;90:197–204.
[12] Donehower LA, Harvey M, Slagle BL, McArthur MJ, Montgomery CA, Butel JS, et al. Mice deficient for p53 are developmentally normal but susceptible to spontaneous tumours. Nature 1992;356:215–21.
[13] Ducharme A, Frantz S, Aikawa M, Rabkin E, Lindsey M, Rohde LE, et al. Targeted deletion of matrix metalloproteinase-9 attenuates left ventricular enlargement and collagen accumulation after experimental myocardial infarction. J Clin Invest 2000;106:55–62.
[14] Shiomi T, Tsutsui H, Hayashidani S, Suematsu N, Ikeuchi M, Wen J, et al. Pioglitazone, a peroxisome proliferator-activated receptor-

gamma agonist, attenuates left ventricular remodeling and failure after experimental myocardial infarction. Circulation 2002;106:3126–32.
[15] Armstrong JF, Kaufman MH, Harrison DJ, Clarke AR. High-frequency developmental abnormalities in p53-deficient mice. Curr Biol 1995;5:931–6.
[16] Rotter V, Schwartz D, Almon E, Goldfinger N, Kapon A, Meshorer A, et al. Mice with reduced levels of p53 protein exhibit the testicular giant-cell degenerative syndrome. Proc Natl Acad Sci U S A 1993;90:9075–9.
[17] Pfeffer MA, Pfeffer JM, Fishbein MC, Fletcher PJ, Spadaro J, Kloner RA, et al. Myocardial infarct size and ventricular function in rats. Circ Res 1979;44:503–12.
[18] Patten RD, Aronovitz MJ, Deras-Mejia L, Pandian NG, Hanak GG, Smith JJ, et al. Ventricular remodeling in a mouse model of myocardial infarction. Am J Physiol 1998;274:H1812–20.
[19] Sam F, Sawyer DB, Chang DL, Eberli FR, Ngoy S, Jain M, et al. Progressive left ventricular remodeling and apoptosis late after myocardial infarction in mouse heart. Am J Physiol Heart Circ Physiol 2000;279:H422–8.
[20] Ikeuchi M, Tsutsui H, Shiomi T, Matsusaka H, Matsushima S, Wen J, et al. Inhibition of TGF-beta signaling exacerbates early cardiac dysfunction but prevents late remodeling after infarction. Cardiovasc Res 2004;64:526–35.
[21] Delyani JA, Robinson EL, Rudolph AE. Effect of a selective aldosterone receptor antagonist in myocardial infarction. Am J Physiol Heart Circ Physiol 2001;281:H647–54.
[22] Lindsey ML, Gannon J, Aikawa M, Schoen FJ, Rabkin E, Lopresti-Morrow L, et al. Selective matrix metalloproteinase inhibition reduces left ventricular remodeling but does not inhibit angiogenesis after myocardial infarction. Circulation 2002;105:753–8.
[23] Hayashidani S, Tsutsui H, Ikeuchi M, Shiomi T, Matsusaka H, Kubota T, et al. Targeted deletion of MMP-2 attenuates early LV rupture and late remodeling after experimental myocardial infarction. Am J Physiol Heart Circ Physiol 2003;285:H1229–35.
[24] Li Q, Li B, Wang X, Leri A, Jana KP, Liu Y, et al. Overexpression of insulin-like growth factor-1 in mice protects from myocyte death after infarction, attenuating ventricular dilation, wall stress, and cardiac hypertrophy. J Clin Invest 1997;100:1991–9.
[25] Bialik S, Geenen DL, Sasson IE, Cheng R, Horner JW, Evans SM, et al. Myocyte apoptosis during acute myocardial infarction in the mouse localizes to hypoxic regions but occurs independently of p53. J Clin Invest 1997;100:1363–72.
[26] Sussman MA, Anversa P. Myocardial aging and senescence: where have the stem cells gone? Annu Rev Physiol 2004;66:29–48.
[27] Nakajima H, Nakajima HO, Tsai SC, Field LJ. Expression of mutant p193 and p53 permits cardiomyocyte cell cycle reentry after myocardial infarction in transgenic mice. Circ Res 2004;94:1606–14.
[28] von Harsdorf R, Li PF, Dietz R. Signaling pathways in reactive oxygen species-induced cardiomyocyte apoptosis. Circulation 1999; 99:2934–41.
[29] Maggioni AP, Maseri A, Fresco C, Franzosi MG, Mauri F, Santoro E, et al. Age-related increase in mortality among patients with first myocardial infarctions treated with thrombolysis. The Investigators of the Gruppo Italiano per lo Studio della Sopravvivenza nell'Infarto Miocardico (GISSI-2). N Engl J Med 1993;329:1442–8.

Targeted Deletion of Matrix Metalloproteinase 2 Ameliorates Myocardial Remodeling in Mice With Chronic Pressure Overload

Hidenori Matsusaka, Tomomi Ide, Shouji Matsushima, Masaki Ikeuchi, Toru Kubota, Kenji Sunagawa, Shintaro Kinugawa, Hiroyuki Tsutsui

Abstract—Matrix metalloproteinases (MMPs) play an important role in the extracellular matrix remodeling. Experimental and clinical studies have demonstrated that MMP 2 and 9 are upregulated in the dilated failing hearts and involved in the development and progression of myocardial remodeling. However, little is known about the role of MMPs in mediating adverse myocardial remodeling in response to chronic pressure overload (PO). We, thus, hypothesized that selective disruption of the MMP 2 gene could ameliorate PO-induced cardiac hypertrophy and dysfunction in mice. PO hypertrophy was induced by transverse aortic constriction (TAC) in male MMP 2 knockout (KO) mice (n=10) and sibling wild-type (WT) mice (n=9). At 6 weeks, myocardial MMP 2 zymographic activity was 2.4-fold increased in WT+TAC, and this increase was not observed in KO+TAC, with no significant alterations in other MMPs (MMP 1, 3, 8, and 9) or tissue inhibitors of MMPs (1, 2, 3, and 4). TAC resulted in a significant increase in left ventricular (LV) weight and LV end-diastolic pressure (EDP) with preserved systolic function. KO+TAC mice exerted significantly lower LV weight/body weight (4.2±0.2 versus 5.0±0.2 mg/g; $P<0.01$), lung weight/body weight (4.9±0.2 versus 6.2±0.4 mg/g; $P<0.01$), and LV end-diastolic pressure (4±1 versus 10±2 mm Hg; $P<0.05$) than WT+TAC mice despite comparable aortic pressure. KO+TAC mice had less myocyte hypertrophy (cross-sectional area; 322±14 versus 392±14 μm^2; $P<0.01$) and interstitial fibrosis (collagen volume fraction; 3.3±0.5 versus 8.2±1.0%; $P<0.01$) than WT+TAC mice. MMP 2 plays an important role in PO-induced LV hypertrophy and dysfunction. The inhibition of MMP 2 activation may, therefore, be a useful therapeutic strategy to manage hypertensive heart disease. (***Hypertension.* 2006;47:711-717.**)

Key Words: hypertrophy ■ heart failure ■ fibrosis ■ extracellular matrix ■ hypertension, experimental ■ myocardium

Left ventricular (LV) hypertrophy is an adaptive process that compensates for pressure overload (PO) caused by hypertension or valvular heart disease, such as aortic stenosis. This remodeling process consists of hypertrophic changes of cardiac myocytes and abnormalities of the extracellular matrix (ECM) network, which are both responsible for changes in systolic and diastolic function.[1]

The dynamic synthesis and breakdown of ECM proteins play an important role in adverse myocardial remodeling. In particular, the increased expression and activation of the matrix metalloproteinases (MMPs) have been shown in various forms of heart failure and implicated in the process of myocardial remodeling that is characteristic of developing heart failure.[2] Despite a number of studies implicating MMPs in cardiac pathophysiology, little is known about the role of MMP in the development of myocardial remodeling in response to chronic PO. MMP 2 and 9 expression has been shown to be enhanced in pressure-overloaded cardiac hypertrophy in spontaneously hypertensive rats[3] and in Dahl salt-sensitive hypertensive rats.[4] Similar upregulation of MMPs has been also observed in human pressure-overloaded hearts because of aortic stenosis.[5] Recently, Heymans et al[6] have demonstrated that MMP 9 is involved in cardiac remodeling associated with hypertension. However, MMP-9 is mainly expressed in such infiltrating inflammatory cells as neutrophils and macrophages.[7] Conversely, MMP 2 is ubiquitously distributed in cardiac myocytes and fibroblasts.[8] Therefore, MMP 2 may also play an important role in the development and progression of myocardial remodeling in response to PO. However, no previous studies have yet determined the pathophysiological significance of MMP 2 in this disease state.

In the present study, we evaluated the effects of a targeted deletion of the MMP 2 gene on both LV structural and

Received November 28, 2005; first decision December 13, 2005; revision accepted January 3, 2006.

From the Department of Cardiovascular Medicine (H.M., T.I., S.M., M.I., T.K., K.S.), Graduate School of Medical Sciences, Kyushu University, Fukuoka; and Department of Cardiovascular Medicine (S.K., H.T.), Hokkaido University Graduate School of Medicine, Sapporo, Japan.

Correspondence to Hiroyuki Tsutsui, Dept of Cardiovascular Medicine, Hokkaido University Graduate School of Medicine, Kita-15, Nishi-7, Kita-ku, Sapporo 060-8638, Japan. E-mail htsutsui@med.hokudai.ac.jp

Hypertension **is available at http://www.hypertensionaha.org** **DOI: 10.1161/01.HYP.0000208840.30778.00**

functional alterations during pressure-overloaded cardiac hypertrophy. To ensure selective and long-term complete inhibition of MMP 2, we used MMP 2 knockout (KO) mice.[9–11] The most effective way to evaluate the contribution of the specific MMP and obtain the direct evidence for a role of MMP is through gene manipulation instead of MMP inhibitor.

Methods

Experimental Animals

The study was approved by our Institutional Animal Research Committee and conformed to the animal care guidelines of the American Physiological Society. We used the progeny of homozygous breeding pairs of C57BL/6J mice with targeted disruption of MMP 2 ranging in age from 11 to 14 weeks old.[10] The mutation heterozygous mice were obtained by crossing the chimeras to C57BL/6J mice. Heterozygotes were backcrossed to C57BL/6J 1 to 5 times and then crossed to obtain the mutation homozygous mice. The original breeding pairs used to develop the mice for this study were obtained from Dr Shigeyoshi Itohara (Laboratory for Behavioral Genetics, RIKEN, Tsukuba, Japan).

Transverse Aortic Constriction

Transverse aortic constriction (TAC) was performed in male MMP 2 KO and sibling wild-type (WT) mice as described previously.[12] Briefly, after anesthetizing by tribromoethanol/amylene hydrate (Avertin; 2.5% weight/volume, 8 μL/g IP), mice were intubated and ventilated, and a thoracotomy was performed via the second intercostal space at the left upper sternal border. The transverse aortic arch was ligated between the innominate and left common carotid arteries with an overlying 28-gauge needle, which, after removal of the needle, left a reproducible discrete region of stenosis. Sham-operated mice underwent a similar procedure without ligation of the aorta.

Tail clips and a PCR protocol to confirm the genotype were performed by a group of investigators. Next, TAC was induced in these mice by another subset of investigators, who were not informed of the genotyping results. This assignment procedure was performed using numeric codes to identify the animals.

MMPs and Tissue Inhibitors of MMPs

First, the myocardial MMP levels, including MMP 2 and MMP 9, were determined in the left ventricle (LV) using gelatin zymography as described previously.[13] The LV myocardial samples were homogenized (≈30-s bursts) in 1 mL of an ice-cold extraction buffer containing cacodylic acid (10 mmol/L), NaCl (0.15 mol/L), $ZnCl_2$ (20 mmol/L), NaN_2 (1.5 mmol/L), and 0.01% Triton X-100 (pH 5.0). The homogenate was then centrifuged (4°C, 10 minutes, 10 000*g*) and the supernatant decanted and saved on ice. The pH levels of the samples were adjusted to 7.5 using Tris (1 mol/L). The final protein concentration of the myocardial extracts was determined using a standardized colorimetric assay. The extracted samples were then aliquoted and stored at −80°C until the time of assay. The myocardial extracts were then directly loaded onto electrophoretic gels (SDS-PAGE) containing 1 mg/mL of gelatin under nonreducing conditions. The myocardial extracts at a final protein content of 5 μg were loaded onto the gels using a 3:1 sample buffer (10% SDS, 4% sucrose, 0.25 mol/L Tris-Cl, and 0.1% bromophenol blue ≤pH 6.8]). The gels were run at 15 mA/gel through the stacking phase (4%) and at 20 mA/gel for the separating phase (10%), whereas the running buffer temperature was maintained at 4°C. After SDS-PAGE, the gels were washed twice in 2.5% Triton X-100 for 30 minutes each, rinsed in water, and incubated for 24 hours in a substrate buffer at 37°C (50 mmol/L Tris-HCl, 5 mmol/L, $CaCl_2$, and 0.02% NaN_3 [pH 7.5]). After incubation, the gels were stained with Coomassie brilliant blue R-250. The zymograms were digitized, and the size-fractionated bands, which indicated the MMP proteolytic levels, were measured by the integrated optical density in a rectangular region of interest.

Next, the mRNA levels of myocardial MMPs including MMP 1, 2, 3, 8, and 9 as well as tissue inhibitors of MMPs (TIMPs) including TIMP 1, 2, 3, and 4 were determined by multiprobe ribonuclease protection assay (RiboQuant, PharMingen). Each value was normalized to that of glyceraldehydes-3-phosphate-dehydrogenase in each template set as an internal control, followed by calculation as a ratio to WT+Sham. The amount of tissue was limited in mice and, thus, tissue needed to be divided so that all of the biochemical analyses could be performed.

Echocardiographic and Hemodynamic Measurements

Echocardiographic studies were performed under light anesthesia with tribromoethanol/amylene hydrate (Avertin; 2.5% weight/volume, 8 μL/g IP) and spontaneous respiration as described previously.[14] A 2D parasternal short-axis view of the LV was obtained at the level of the papillary muscles. In general, the best views were obtained with the transducer lightly applied to the mid-upper left anterior chest wall. The transducer was then gently moved cephalad or caudad and angulated until desirable images were obtained. After confirming that the imaging was on axis (based on roundness of the LV cavity), 2D targeted M-mode tracings were recorded at a paper speed of 50 mm/s. Two consecutive heartbeats of each frame were analyzed to measure the wall thickness and end-diastolic (EDD) and end-systolic (ESD) internal dimensions of the LV. LV fractional shortening (FS) was calculated as LV EDD minus LV ESD normalized for LV EDD and was taken as an index of LV systolic performance. Echocardiographic LV mass was calculated according to the standard cube formula as described previously.[15] Our previous validation study has shown that the intraobserver and interobserver variabilities of our echocardiographic measurements for LV cavity dimensions and FS were small, and measurements made in the same animals on separate days were highly reproducible.[14] Next, a 1.4-Fr micromanometer-tipped catheter (Millar) was inserted into the right carotid artery and then was advanced into the LV to measure the LV pressures. Arterial blood pressure and heart rate were also measured with the use of a noninvasive tail-cuff system (BP-98A, Softron).[16]

Organ Weight and Histopathology

After in vivo echocardiographic and hemodynamic studies, the heart and lung were excised, and their weights were determined. The heart was dissected into the right and left ventricles, including the septum. From the mid-LV transverse sections, 5-μm sections were cut and stained with hematoxylin/eosin and Masson's trichrome to determine the myocyte cross-sectional area and collagen volume fraction. To measure the myocyte cross-sectional area, each section was photographed using a microscope and magnified (final magnification: ×750). Connective tissue and muscle areas were identified, and the profile margin of 30 to 40 myocytes cut into cross-sections was manually traced and digitized. The digitized profiles were transferred to a personal computer that calculated the area. Three to 4 fields were randomly selected from 2 to 3 coronal sections of each heart. Thus, ≈100 to 200 myocytes were measured for each animal, and the mean myocyte cross-sectional area was calculated.[17] Collagen volume fraction was measured at ≈5 to 7 fields for each heart.[18] Within each field, segments representing connective tissue and myocyte were identified and manually traced by using a digitizing pad with a computer to calculate the traced area. Collagen volume fraction was then calculated for the heart as the sum of all of the connective tissue areas divided by the sum of all of the connective tissue and muscle areas in all fields. Collagen surrounding intramyocardial coronary arteries was excluded from the analysis.

Statistical Analysis

All of the data are expressed as the mean±SEM. Between-group comparisons of the means were performed by 1-way ANOVA, followed by *t* tests. The Bonferroni's correction was done for multiple comparisons of the means.

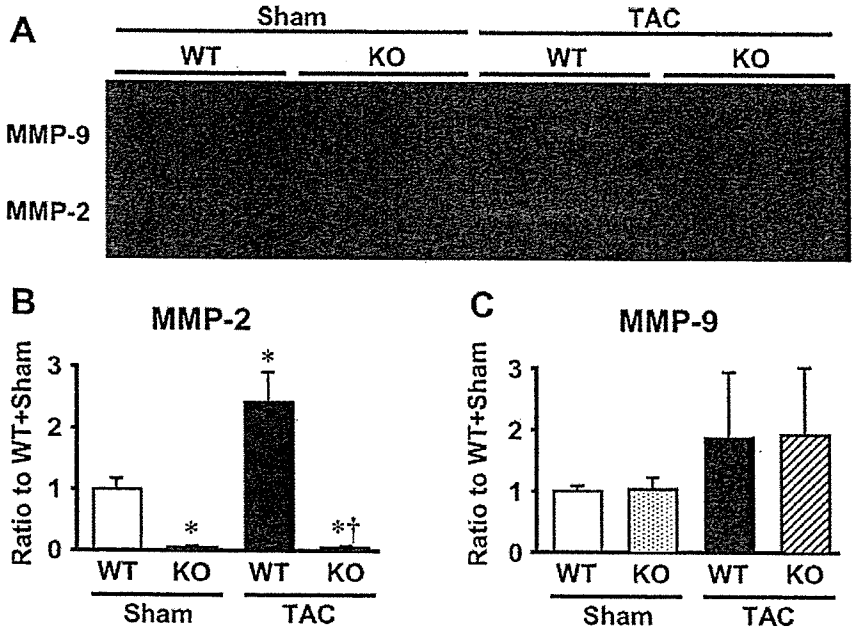

Figure 1. (A) Representative gelatin zymography of the LV from 4 groups of WT+Sham, KO+Sham, WT+TAC, and KO+TAC mice. (B and C) Densitometric analysis of MMP-2 (B) and MMP-9 (C) zymographic activity (n=3 each). Data are expressed as the ratio to WT+Sham values run concurrently on the same gel. Values are mean±SEM. *$P<0.05$ vs WT+Sham; †$P<0.01$ vs WT+TAC.

Results

MMPs and TIMPs

At 6 weeks of TAC, the zymographic MMP 2 levels increased by 2.4-fold compared with WT+Sham mice (Figure 1). As expected, MMP 2 activity was not detected in KO+Sham and KO+TAC mice. Importantly, the MMP 9 zymographic levels did not differ between WT+TAC and KO+TAC.

Again, the MMP 2 mRNA levels significantly increased in the WT+TAC compared with WT+Sham (Figure 2). This increase was not observed in KO+TAC. These results were consistent with those observed in gelatin zymography (Figure 1). Other MMPs, including MMP 1, 3, 8, and 9, were not altered in these mice (Figure 2). The changes of TIMPs (TIMP 1, 2, 3, and 4) were also comparable between WT+TAC and KO+TAC.

Echocardiography

The presence or absence of MMP 2 gene did not affect baseline heart rate or echocardiographic parameters in Sham mice (Table 1). TAC significantly increased LV wall thickness (Table 1) and echocardiographic LV mass (Figure 3) without affecting LV diameters or FS in WT+TAC. These LV hypertrophic changes in WT+TAC were significantly ameliorated in KO+TAC.

Hemodynamics

LV systolic pressure was markedly elevated by TAC (Table 2). However, there was no significant difference in LV systolic pressure between WT+TAC and KO+TAC mice. LV EDP increased significantly in WT+TAC mice, and this increase was significantly attenuated in KO+TAC mice.

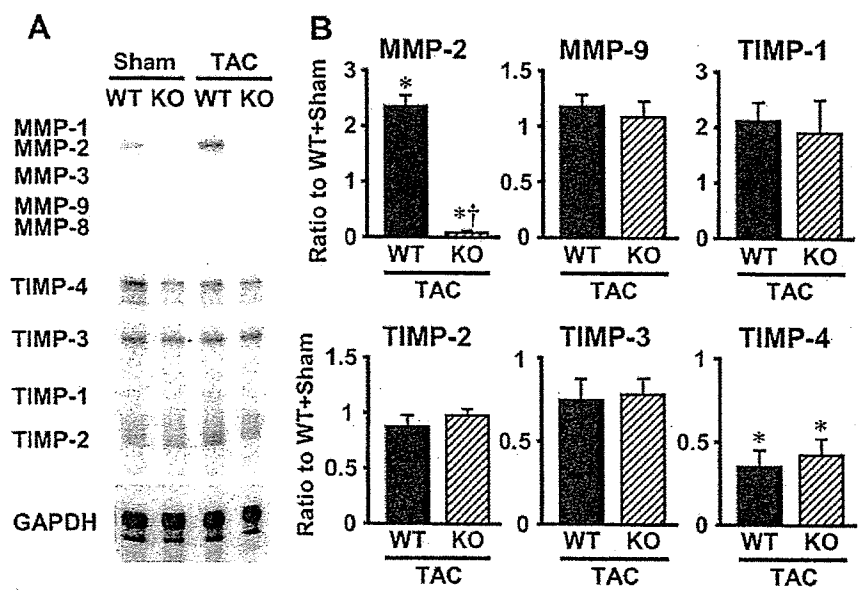

Figure 2. (A) Representative image of myocardial gene expression of MMPs and TIMPs. (B) Densitometric analysis of MMP and TIMP gene expression from WT+TAC (n=5) and KO+TAC (n=4). Each value was normalized to that of glyceraldehydes-3-phosphate-dehydrogenase in each template set as an internal control and expressed as the ratio to WT+Sham (n=3). Values are mean±SEM. *$P<0.01$ vs WT+Sham; †$P<0.01$ vs WT+TAC.

TABLE 1. Echocardiographic Data

Variable	WT+Sham (n=6)	KO+Sham (n=6)	WT+TAC (n=9)	KO+TAC (n=10)
Heart rate, bpm	469±10	467±13	475±8	470±6
LV EDD, mm	3.6±0.1	3.6±0.1	3.7±0.1	3.6±0.1
LV ESD, mm	2.2±0.1	2.2±0.1	2.4±0.1	2.3±0.1
Fractional shortening, %	37.2±0.8	36.3±1.0	35.1±0.9	35.5±0.7
Anterior wall thickness, mm	0.70±0.03	0.70±0.03	0.99±0.02*†	0.84±0.03*†‡
Posterior wall thickness, mm	0.77±0.02	0.78±0.02	1.04±0.02*†	0.92±0.03*†‡

Sham indicates sham operation without ligation of the aorta. Values are mean±SEM.
*P<0.01 vs WT+Sham; †P<0.01 vs KO+Sham; ‡P<0.01 vs WT+TAC.

Organ Weights

In agreement with echocardiographic LV mass (Figure 3), TAC increased LV weight in WT mice (Figure 4A). Furthermore, in accordance with LV EDP, lung weight/body weight, indicative of pulmonary congestion, increased significantly in WT+TAC (Figure 4B). In KO+TAC, both increased LV and lung weights were significantly reduced.

Histopathology

Masson's trichrome staining showed the increase in myocyte size and interstitial collagen volume fraction in WT+TAC mice compared with WT+Sham mice (Figure 5). The selective disruption of the MMP 2 gene significantly ameliorated myocyte hypertrophy and interstitial fibrosis by TAC. Similarly, picrosirius staining also demonstrated collagen deposition in the interstitial areas in LV sections from WT+TAC mice and the amelioration of interstitial fibrosis in KO+TAC mice (data not shown).

Discussion

In the present study, we demonstrated that the selective disruption of the MMP 2 gene ameliorated LV remodeling, such as myocyte hypertrophy and interstitial fibrosis in TAC mice, thus providing direct evidence that MMP 2 is involved in mediating PO-induced cardiac hypertrophy. These beneficial effects of MMP 2 inhibition occurred without affecting hemodynamics.

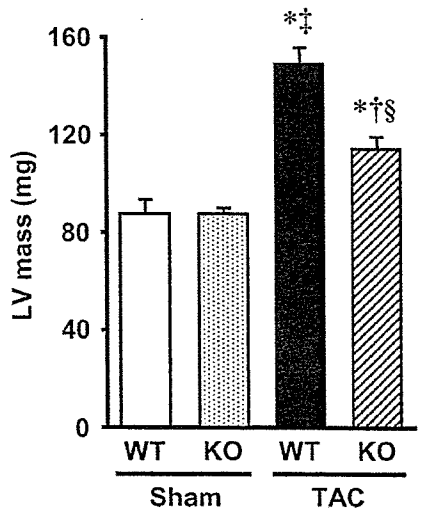

Figure 3. Echocardiographic LV mass from 4 groups of WT+Sham (n=6), KO+Sham (n=6), WT+TAC (n=9), and KO+TAC (n=10) mice. Values are mean±SEM. *P<0.01 vs WT+Sham; †P<0.05, ‡P<0.01 vs KO+Sham; §P<0.01 vs WT+TAC.

Upregulation of MMP 2 in PO Hypertrophy

The present study demonstrated that the MMP 2 gene expression and gelatinolytic activities were upregulated in the myocardium during PO (Figures 1 and 2). These findings, coupled with past reports, suggest that an increase in myocardial MMP levels is a fairly uniform event in myocardial remodeling.[2,3,6,19,20] Although the mechanisms responsible for this activation remain to be determined, cellular constituents of cardiac muscle, including fibroblasts, inflammatory cells, and myocytes, are known to be capable of expressing MMP 2 in response to specific stimuli, including mechanical stress.[9,21]

Role of MMP 2 in PO Hypertrophy

Alterations in the expression and activity of MMP 2 have been demonstrated in a number of pathophysiological conditions, such as myocardial infarction (MI) and heart failure. Our previous study[10] and a recent study by Matsumura et al[22] have demonstrated that the inhibition of MMP 2 activity improves the survival rate after acute MI by preventing cardiac rupture and delays after MI remodeling. A recent study by Wang et al[23] has shown that cardiac-specific, constitutively active MMP 2 expression leads to impaired contraction and diminished responses to inotropic stimulation, indicating that MMP 2 can directly impair cardiac function in the absence of superimposed injury.

Broad-spectrum pharmacological inhibition of MMPs significantly attenuated myocardial remodeling associated with chronic volume overload[3] or hypertension.[19] However, the most effective way to evaluate the contribution of the specific MMP and to obtain the direct evidence for a role of MMP in myocardial remodeling and failure is through such gene manipulation as that used in the present study. As expected, no MMP 2 expression was observed in the myocardium from KO mice in this study (Figures 1 and 2). Thus, the present study could investigate the effects of selective disruption of the MMP 2 gene on the development of myocardial hypertrophy induced by PO.

The most striking finding of the present study was the inhibition of myocardial hypertrophy in MMP 2 KO mice

TABLE 2. Hemodynamic Data

Variable	WT+Sham (n=6)	KO+Sham (n=6)	WT+TAC (n=9)	KO+TAC (n=10)
Heart rate, bpm	503±3	504±5	507±6	512±6
Arterial blood pressure, mm Hg	73±2	76±5	74±2	71±2
LV systolic pressure, mm Hg	104±4	104±3	202±6*†	196±9*†
LVEDP, mm Hg	1.5±1.2	2.4±0.9	9.8±2.2*†	3.5±0.7‡

Sham indicates sham operation without ligation of the aorta. Values are mean±SEM.
*P<0.01 vs WT+Sham; †P<0.01 vs KO+Sham; ‡P<0.05 vs WT+TAC.

under PO (Figures 3 through 5). Our previous studies demonstrated the beneficial effects of MMP 2 deletion also on postinfarct LV remodeling and failure.[10] Similar to the present study, both myocyte hypertrophy and interstitial collagen accumulation were ameliorated in the MMP 2–deficient mice after MI. Moreover, the present study is consistent with previous studies from other laboratories, which demonstrated the involvement of myocardial MMP in heart failure.[2,24,25] Therefore, the present study builds on these past reports by demonstrating that MMP inhibition attenuated myocardial remodeling that occurred also under PO.

The present study demonstrated that increased MMP 2 activity was associated with the interstitial fibrosis in pressure-overloaded LV and the selective inhibition of MMP 2, indeed, ameliorated these changes (Figure 5). Theoretically, an increase in MMP activity would result in a decrease in the MMP substrate, collagens, whereas an inhibition of MMP would result in an increase in collagens. However, in agreement with previous studies,[10] an increase in MMP 2 activity was accompanied by increased fibrosis in our model of LV hypertrophy, which is probably because of the direct proteolysis of myocardial matrix components, as well as by facilitating a profibrotic response. In fact, the selective disruption of the MMP 2 gene did attenuate interstitial fibrosis. Although the present study could not provide the definite explanation for these paradoxical findings, this might be because of the fact that the total ECM collagen content is a complex function of both synthesis and degradation.

In addition to interstitial fibrosis, myocyte cellular hypertrophy was also ameliorated by the selective blockade of the MMP 2 gene (Figure 5), suggesting that myocardial induction of MMP 2 is involved in the development of myocyte hypertrophy during PO. Recently, Heymans et al[6] demonstrated that MMP 9 gene inactivation reduced hypertrophic changes in cardiac myocytes during acute PO. These results suggest that there is an intimate link between MMPs and the myocyte hypertrophic process, which might be mediated, at least in part, by the tissue infiltration of inflammatory cells. However, the precise role of MMPs in the development of myocyte hypertrophy has not been fully explored. MMPs may be involved in a complex myocyte–matrix interaction, because the basement membrane components, collagen IV and laminin, are the substrates for MMP 2 and MMP 9.[26] Thus, increased MMP 2 activity within the myocardium can contribute to the discontinuity of the basement membrane, thereby disrupting the normal myocyte-matrix interface. The findings that MMP inhibition limited the degree of myocyte hypertrophy raise an issue requiring additional studies.

Limitations

There are several issues to be acknowledged as a limitation in this study. First, although in vivo assessment of LV function with echocardiography is feasible and reproducible in the mouse, it might still be difficult to interpret the indices of LV function. However, our validation study has shown that the intraobserver and interobserver variabilities of our echocar-

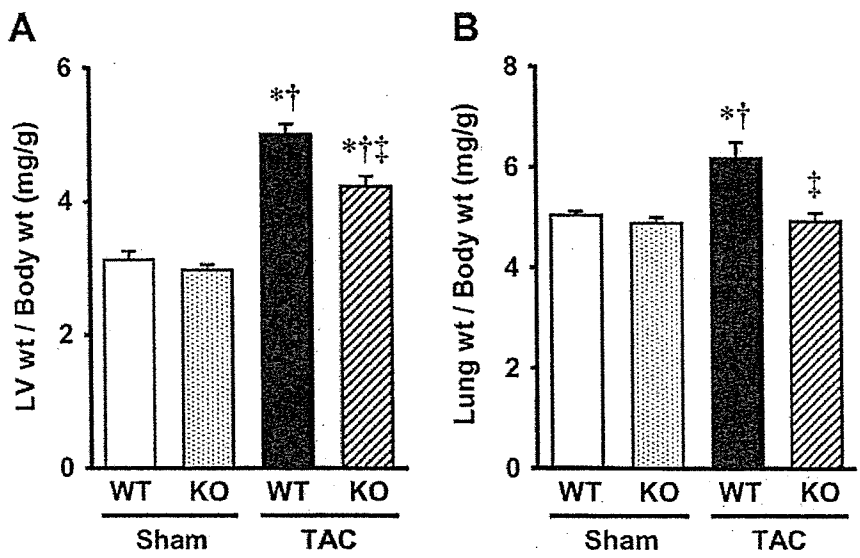

Figure 4. LV weight and lung weight from 4 groups of WT+Sham (n=6), KO+Sham (n=6), WT+TAC (n=9), and KO+TAC (n=10) mice. Values are mean±SEM. *P<0.01 vs WT+Sham; †P<0.01 vs KO+Sham; ‡P<0.01 vs WT+TAC.

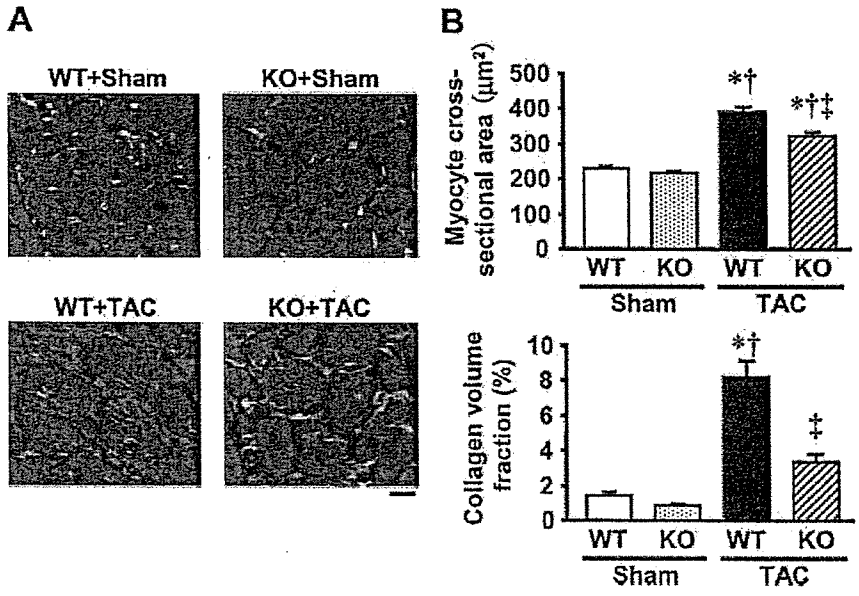

Figure 5. (A) Representative high-power photomicrographs of LV cross-sections stained with Masson's trichrome from 4 groups of WT+Sham, KO+Sham, WT+TAC, and KO+TAC mice. Scale bar, 10 μm. (B) Summary data of myocyte cross-sectional area (top) and collagen volume fraction (bottom) by the histomorphometric analysis of LV tissue sections from 4 groups of WT+Sham (n=4), KO+Sham (n=4), WT+TAC (n=5), and KO+TAC (n=5) mice. Values are mean±SEM. *$P<0.01$ vs WT+Sham; †$P<0.01$ vs KO+Sham; ‡$P<0.01$ vs WT+TAC.

diographic measurements for LV dimensions and FS were small, and the measurements made in the same animals on separate days were highly reproducible.[14] Therefore, our technique could be considered to allow for a noninvasive assessment of the LV structure and function. Second, the heart rate values in the present study (460 to 480 bpm) were lower than those (600 bpm) measured in conscious mice. Therefore, the LV size and function data might be greatly influenced by differences in anesthetic regimens and the experimental conditions, such as the heart rate. Third, MMP 9 was not increased in our model of PO hypertrophy. Although the present study could not provide the definite explanation for these results, they might be related to the small number of infiltrating inflammatory cells as neutrophils and macrophages, in which MMP 9 is mainly expressed, within the hypertrophied LV.

Perspectives

Diastolic dysfunction is an important factor contributing to the development of heart failure. One of the most common causes for diastolic heart failure is LV hypertrophy associated with hypertension. The present study demonstrated that MMP 2 inhibition reduced myocyte hypertrophy and interstitial fibrosis, which might contribute to a decrease in LV EDP and lung weight, an index of pulmonary congestion, without affecting LV systolic function. Therefore, although the present study did not directly evaluate the diastolic function itself, the reduction of LV EDP and lung congestion achieved with MMP 2 inhibition in this model is considered to be because of the attenuation of LV hypertrophy and the resultant improvement of diastolic function.

Conclusions

Chronic PO results in an initial cardiac hypertrophic response followed by progressive failure. Our findings provide the first direct evidence that MMP 2 is involved in mediating the adverse myocardial remodeling that occurs in response to a common form of hemodynamic overload. The beneficial effects of MMP 2 inhibition occurred in the absence of a decrease in systemic blood pressure. These findings suggest that the early institution of MMP 2 inhibition may have use in preventing the development of maladaptive myocardial remodeling in response to hypertension.

Acknowledgments

This study was supported in part by grants from the Ministry of Education, Science and Culture (No. 12670676, 14370230, and 17390223). A part of this study was conducted in Kyushu University Station for Collaborative Research I and II.

References

1. Redfield MM, Jacobsen SJ, Burnett JC Jr, Mahoney DW, Bailey KR, Rodeheffer RJ. Burden of systolic and diastolic ventricular dysfunction in the community: appreciating the scope of the heart failure epidemic. *JAMA*. 2003;289:194–202.
2. Spinale FG. Matrix metalloproteinases: regulation and dysregulation in the failing heart. *Circ Res*. 2002;90:520–530.
3. Peterson JT, Hallak H, Johnson L, Li H, O'Brien PM, Sliskovic DR, Bocan TM, Coker ML, Etoh T, Spinale FG. Matrix metalloproteinase inhibition attenuates left ventricular remodeling and dysfunction in a rat model of progressive heart failure. *Circulation*. 2001;103:2303–2309.
4. Sakata Y, Yamamoto K, Mano T, Nishikawa N, Yoshida J, Hori M, Miwa T, Masuyama T. Activation of matrix metalloproteinases precedes left ventricular remodeling in hypertensive heart failure rats: its inhibition as a primary effect of Angiotensin-converting enzyme inhibitor. *Circulation*. 2004;109:2143–2149.
5. Polyakova V, Hein S, Kostin S, Ziegelhoeffer T, Schaper J. Matrix metalloproteinases and their tissue inhibitors in pressure-overloaded human myocardium during heart failure progression. *J Am Coll Cardiol*. 2004;44:1609–1618.
6. Heymans S, Lupu F, Terclavers S, Vanwetswinkel B, Herbert JM, Baker A, Collen D, Carmeliet P, Moons L. Loss or inhibition of uPA or MMP-9 attenuates LV remodeling and dysfunction after acute pressure overload in mice. *Am J Pathol*. 2005;166:15–25.
7. Romanic AM, Harrison SM, Bao W, Burns-Kurtis CL, Pickering S, Gu J, Grau E, Mao J, Sathe GM, Ohlstein EH, Yue TL. Myocardial protection from ischemia/reperfusion injury by targeted deletion of matrix metalloproteinase-9. *Cardiovasc Res*. 2002;54:549–558.
8. Cheung PY, Sawicki G, Wozniak M, Wang W, Radomski MW, Schulz R. Matrix metalloproteinase-2 contributes to ischemia-reperfusion injury in the heart. *Circulation*. 2000;101:1833–1839.
9. Schubert A, Walther T, Falk V, Binner C, Loscher N, Kanev A, Bleiziffer S, Rauch T, Autschbach R, Mohr FW. Extracellular matrix gene expression correlates to left ventricular mass index after surgical

induction of left ventricular hypertrophy. *Basic Res Cardiol.* 2001;96: 381–387.
10. Hayashidani S, Tsutsui H, Ikeuchi M, Shiomi T, Matsusaka H, Kubota T, Imanaka-Yoshida K, Itoh T, Takeshita A. Targeted deletion of MMP-2 attenuates early LV rupture and late remodeling after experimental myocardial infarction. *Am J Physiol Heart Circ Physiol.* 2003;285: H1229–H1235.
11. Itoh T, Ikeda T, Gomi H, Nakao S, Suzuki T, Itohara S. Unaltered secretion of β-amyloid precursor protein in gelatinase A (matrix metalloproteinase 2)-deficient mice. *J Biol Chem.* 1997;272:22389–22392.
12. Rockman HA, Ross RS, Harris AN, Knowlton KU, Steinhelper ME, Field LJ, Ross J Jr, Chien KR. Segregation of atrial-specific and inducible expression of an atrial natriuretic factor transgene in an in vivo murine model of cardiac hypertrophy. *Proc Natl Acad Sci USA.* 1991;88: 8277–8281.
13. Matsusaka H, Ikeuchi M, Matsushima S, Ide T, Kubota T, Feldman AM, Takeshita A, Sunagawa K, Tsutsui H. Selective disruption of MMP-2 gene exacerbates myocardial inflammation and dysfunction in mice with cytokine-induced cardiomyopathy. *Am J Physiol Heart Circ Physiol.* 2005;289:H1858–H1864.
14. Shiomi T, Tsutsui H, Hayashidani S, Suematsu N, Ikeuchi M, Wen J, Ishibashi M, Kubota T, Egashira K, Takeshita A. Pioglitazone, a peroxisome proliferator-activated receptor-γ agonist, attenuates left ventricular remodeling and failure after experimental myocardial infarction. *Circulation.* 2002;106:3126–3132.
15. Liao Y, Ishikura F, Beppu S, Asakura M, Takashima S, Asanuma H, Sanada S, Kim J, Ogita H, Kuzuya T, Node K, Kitakaze M, Hori M. Echocardiographic assessment of LV hypertrophy and function in aortic-banded mice: necropsy validation. *Am J Physiol Heart Circ Physiol.* 2002;282:H1703–H1708.
16. Krege JH, Hodgin JB, Hagaman JR, Smithies O. A noninvasive computerized tail-cuff system for measuring blood pressure in mice. *Hypertension.* 1995;25:1111–1115.
17. Ishibashi Y, Tsutsui H, Yamamoto S, Takahashi M, Imanaka-Yoshida K, Yoshida T, Urabe Y, Sugimachi M, Takeshita A. Role of microtubules in myocyte contractile dysfunction during cardiac hypertrophy in the rat. *Am J Physiol.* 1996;271:H1978–H1987.
18. Namba T, Tsutsui H, Tagawa H, Takahashi M, Saito K, Kozai T, Usui M, Imanaka-Yoshida K, Imaizumi T, Takeshita A. Regulation of fibrillar collagen gene expression and protein accumulation in volume-overloaded cardiac hypertrophy. *Circulation.* 1997;95:2448–2454.
19. Chancey AL, Brower GL, Peterson JT, Janicki JS. Effects of matrix metalloproteinase inhibition on ventricular remodeling due to volume overload. *Circulation.* 2002;105:1983–1988.
20. Heymans S, Schroen B, Vermeersch P, Milting H, Gao F, Kassner A, Gillijns H, Herijgers P, Flameng W, Carmeliet P, Van de Werf F, Pinto YM, Janssens S. Increased cardiac expression of tissue inhibitor of metalloproteinase-1 and tissue inhibitor of metalloproteinase-2 is related to cardiac fibrosis and dysfunction in the chronic pressure-overloaded human heart. *Circulation.* 2005;112:1136–1144.
21. Nagatomo Y, Carabello BA, Coker ML, McDermott PJ, Nemoto S, Hamawaki M, Spinale FG. Differential effects of pressure or volume overload on myocardial MMP levels and inhibitory control. *Am J Physiol Heart Circ Physiol.* 2000;278:H151–H161.
22. Matsumura S, Iwanaga S, Mochizuki S, Okamoto H, Ogawa S, Okada Y. Targeted deletion or pharmacological inhibition of MMP-2 prevents cardiac rupture after myocardial infarction in mice. *J Clin Invest.* 2005; 115:599–609.
23. Wang GY, Bergman MR, Nguyen AP, Turcato S, Swigart PM, Rodrigo MC, Simpson PC, Karliner JS, Lovett DH, Baker AJ. Cardiac transgenic matrix metalloproteinase-2 expression directly induces impaired contractility. *Cardiovasc Res.* 2006;69:688–696.
24. Heymans S, Luttun A, Nuyens D, Theilmeier G, Creemers E, Moons L, Dyspersin GD, Cleutjens JP, Shipley M, Angellilo A, Levi M, Nube O, Baker A, Keshet E, Lupu F, Herbert JM, Smits JF, Shapiro SD, Baes M, Borgers M, Collen D, Daemen MJ, Carmeliet P. Inhibition of plasminogen activators or matrix metalloproteinases prevents cardiac rupture but impairs therapeutic angiogenesis and causes cardiac failure. *Nat Med.* 1999;5:1135–1142.
25. Ducharme A, Frantz S, Aikawa M, Rabkin E, Lindsey M, Rohde LE, Schoen FJ, Kelly RA, Werb Z, Libby P, Lee RT. Targeted deletion of matrix metalloproteinase-9 attenuates left ventricular enlargement and collagen accumulation after experimental myocardial infarction. *J Clin Invest.* 2000;106:55–62.
26. Nagase H, Woessner JF Jr. Matrix metalloproteinases. *J Biol Chem.* 1999;274:21491–21494.

Microtubules Modulate the Stiffness of Cardiomyocytes Against Shear Stress

Satoshi Nishimura, Shinya Nagai, Masayoshi Katoh, Hiroshi Yamashita, Yasutake Saeki, Jun-ichi Okada, Toshiaki Hisada, Ryozo Nagai, Seiryo Sugiura

Abstract—Although microtubules are involved in various pathological conditions of the heart including hypertrophy and congestive heart failure, the mechanical role of microtubules in cardiomyocytes under such conditions is not well understood. In the present study, we measured multiple aspects of the mechanical properties of single cardiomyocytes, including tensile stiffness, transverse (indentation) stiffness, and shear stiffness in both transverse and longitudinal planes using carbon fiber–based systems and compared these parameters under control, microtubule depolymerized (colchicine treated), and microtubule hyperpolymerized (paclitaxel treated) conditions. From all of these measurements, we found that only the stiffness against shear in the longitudinal plane was modulated by the microtubule cytoskeleton. A simulation model of the myocyte in which microtubules serve as compression-resistant elements successfully reproduced the experimental results. In the complex strain field that living myocytes experience in the body, observed changes in shear stiffness may have a significant influence on the diastolic property of the diseased heart. (***Circ Res.* 2006;98:81-87.**)

Key Words: cytoskeleton ■ microtubules ■ cardiomyocyte

In mammalian cells, microtubules and actin filaments constitute the major components of the cytoskeleton and participate in a variety of cellular processes, including organelle transport, cell division, and migration as well as maintenance or alteration of the cell morphology in response to mechanical stimuli transmitted from the surrounding extracellular matrix.[1–3] However, in the case of postmitotic adult ventricular cardiomyocytes, the functional significance of microtubules may be somewhat different. Their relative content of microtubules (tubulin) is small compared with other types of cells[4] but increases in various disease conditions, such as cardiac hypertrophy or heart failure, in which the heart is subjected to abnormally high loads.[5,6]

In this context, studies at the tissue (papillary muscle) and cellular levels have focused on the impact of microtubule proliferation on the contractile function of the myocardium, but the results obtained are controversial. The microtubule proliferation observed in hypertrophied hearts was associated with contractile dysfunction and pharmacological disruption of the microtubules by colchicines (COLs) normalized the contractile function.[7,8] However, in the absence of the preceding hypertrophic proliferation of microtubules, COLs do not improve contractile function.[9,10] The structural role of the microtubules has also been evaluated by recording the stress–strain relationship of single cardiomyocytes in the longitudinal direction, but the results failed to establish causality for the stiff passive properties observed in the diseased heart.[11,12] Studies using magnetic twisting cytometry revealed increased cytoskeletal stiffness and viscosity in hypertrophied myocytes with a high microtubule density,[13] but this methodology did not provide any information regarding the anisotropic properties of these polarized cells or allow evaluation of the reported parameters in the complex strain field that living myocytes experience in the body.

The current study investigated the role of microtubules in the cardiac adaptation process by evaluating the structural properties of single rat cardiomyocytes containing variable amounts of microtubules. In addition to ordinary measurements of the stress–strain relationship in the long axis of each myocyte, we also recorded the transverse stiffness and shear stiffness in both the longitudinal and transverse planes. It was found that microtubules modulate the stiffness of cardiomyocyte only against the shear stress in the longitudinal plane. This result can be taken to indicate that microtubules serve as compression-resistant elements as suggested by the cellular tensegrity model.[1] Simulation study based on this model successfully reproduced the experimental findings.

Materials and Methods

An expanded Materials and Methods section is provided in the online data supplement available at http://circres.ahajournals.org.

Original received August 1, 2005; revision received November 15, 2005; accepted November 16, 2005.

From the Department of Cardiovascular Medicine (S. Nishimura, M.K., H.Y., R.N.), Graduate School of Medicine, and The Institute of Environmental Studies (S. Nagai, J.-i.O., T.H., S.S.), Graduate School of Frontier Sciences, The University of Tokyo; and the Department of Physiology (Y.S.), Dental School, Tsurumi University, Japan.

Correspondence to Seiryo Sugiura, Institute of Environmental Studies, Graduate School of Frontier Sciences, The University of Tokyo, Hongo 7-3-1, Bunkyo-ku, Tokyo 113-0033, Japan. E-mail sugiura@k.u-tokyo.ac.jp

Circulation Research **is available at http://circres.ahajournals.org** **DOI: 10.1161/01.RES.0000197785.51819.e8**

Isolation of Cardiomyocytes

Single ventricular myocytes were isolated from 7-week-old female Wistar rats as described previously.[14] We also studied the myocytes from 10-week-old male cardiomyopathic hamsters (Bio TO-2 strain) and age-matched Syrian golden hamsters (Bio-Breeders Institute, Cambridge, Mass). All the experiments were performed at room temperature. All studies were conducted in accordance with the NIH *Guide for the Care and Use of Laboratory Animals* and were approved by the Institutional Animal Care and Use Committee.

Cell Mechanics Measurements

We characterized the mechanical properties of cardiomyocytes in 3 ways, ie, "tensile stiffness," "transverse stiffness," and "shear stiffness." The tensile stiffness was measured using a cell adhesive carbon fiber–based system as described previously.[14,15] Briefly, a rod-shaped quiescent single cardiomyocyte was selected under a microscope and a pair of carbon fibers was attached to both ends using micromanipulators (Figure 1A). One fiber was compliant, whereas the other was thick and rigid and served as a mechanical anchor. The position of the compliant fiber was controlled by a piezoelectric translator (PZT; P-841.40; Physik Instrumente, Karlsruhe, Germany) by a personal computer, and the position of the free end (attached to the cell) was monitored by projecting its image onto a linear photodiode array (S3903; Hamamatsu Photonics, Hamamatsu City, Japan).[14] The sarcomere length was simultaneously measured by real-time fast Fourier transform analysis of the striation pattern (IonOptix, Milton, Mass). To measure the tensile stiffness, the cell was stretched at a strain rate of 0.01/sec by pulling the attached carbon fibers, and the tensile stress–strain relationship was obtained.

We used the same experimental setup to measure the transverse stiffness, with some modifications. We attached a latex microsphere (diameter: 5 μm; Polysciences, Warrington, Pa) to the side of the tip of the compliant carbon fiber, such that the microsphere could be pushed against the myocyte horizontally (Figure 3A). In each experiment, we selected a myocyte with a rectangular shape, placed it along the sidewall in a glass chamber, and performed an indentation test by moving the compliant fiber (2 μm/sec). Because the area of contact clearly increased during the experiment and this was difficult to quantify, we determined the effective transverse stiffness (*Keff*) by evaluating the slope of the force-indentation curve as the indentation (δ) approached 0[16]:

$$Keff = \frac{\text{applied force}}{\text{indentation}}\Big|_{\delta \to 0}$$

To evaluate the shear stiffness, we held the myocyte between the bottom coverglass and a small thin glass plate at the top. Small pieces of thin glass plates (thickness: 5 μm; Glass Flakes, REF-160; Nippon Sheet Glass, Tokyo, Japan) were precoated with laminin (Sigma, St Louis, Mo). Under a microscope, a selected single piece of an appropriate size to cover the whole cell was glued to the tip of the thin carbon fiber (Aronalpha; TOAGOSEI, Tokyo, Japan) in the experimental chamber consisting of a Plexiglas frame and a laminin-coated coverglass at the bottom. We gently attached the glass plate to the top surface of the cell (Figure 4A and 4B), and the myocyte was placed either parallel or perpendicular to the direction of the applied shear force. A 10% shear strain was applied by shifting the glass flake connected to a piezoelectric translator via the carbon fiber in 10 seconds in both the longitudinal and transverse plan. All the signals were recorded at 1 kHz by a personal computer (PowerLab/8SP; AD Instruments, Castle Hill, NSW, Australia).

Altering the Polymerization State of Microtubules

To alter the polymerization state of microtubules, COL (Sigma) or paclitaxel (PAC) (Sigma) was added to Tyrode solution and incubated before the mechanics measurements.

Immunocytochemical Procedures

The microtubules were immunocytochemically labeled with a monoclonal antibody against tubulin after fixation, and actin was simultaneously stained with rhodamine phalloidin (Invitrogen). The cells were observed using a laser confocal microscopy (CSU21; Yokogawa-Denki, Musashino, Japan).

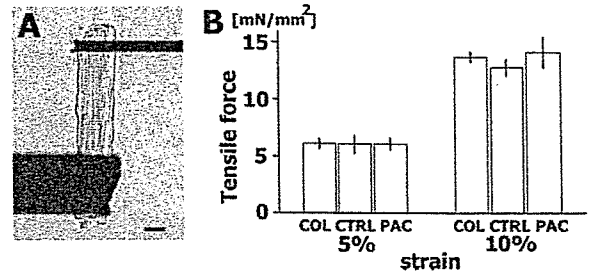

Figure 1. Tensile stiffness. A, Tensile stiffness was evaluated by applying a tensile strain via a pair of carbon fibers. The cell was stretched by displacing the attached carbon fibers using a piezoelectric translator. Scale bar=10 μm. B, The tensile stiffness was calculated from the obtained stress–strain relationship (6.02±0.80 mN/mm² at 5% strain and 12.81±0.73 mN/mm² at 10% strain for CTRL myocytes, n=8). Scale bar=10 μm. The stiffness remains unchanged after treatment with COL (6.07±0.44 mN/mm² at 5% and 13.71±0.45 mN/mm² at 10%, n=10) or PAC (6.04±0.54 mN/mm² at 5% and 14.18±1.36 mN/mm² at 10%, n=10). P=0.99 for group comparisons by ANOVA.

Data Analysis

Results are expressed as the mean±SEM. The statistical significance of the microtubule density for each mechanical property was assessed by ANOVA. If statistically significant differences were discovered, pairwise comparisons (Student's t test) were performed. A probability value of less than 0.05 was considered statistically significant.

Simulation Model

Microtubules, cytoskeletal actin filaments, and desmin filaments (intermediate filaments) were modeled by truss elements (no. 1874) using the Young's moduli and geometrical parameters listed in the supplemental Table.[17–20] Young's modulus of microtubule has been estimated by either applying bending force to microtubules[18,21,22] or recording thermally induced shape fluctuations (statistical mechanics model).[22,23] From the reported values ranging from 100 MPa to 1.2 GPa, we adopted an intermediate value of 500 MPa, which corresponds to a persistence length of 2200 μm. Myofibrils were modeled as solid elements (no. 21540), the material properties of which were characterized using the anisotropic hyperelasticity proposed by Humphrey et al for cardiac muscle tissue.[24]

Results

Mean sarcomere length of studied rat cardiomyocytes was 1.93±0.08 μm (n=8) before the strain was applied. When tensile stress was applied to a myocyte by pulling a pair of carbon fibers attached to both ends of the cell (Figure 1A), the simultaneously measured sarcomere length changed proportionally to the segment length, demonstrating that the stress was distributed homogeneously along the myocyte. From the stress–strain relationship obtained, the average stiffness value for control (CTRL) myocytes (n=8) under tensile stress was determined to be 6.02±0.80 mN/mm² at 5% strain and 12.81±0.73 mN/mm² at 10% strain (Figure 1B). Visualization of the microtubule density in CTRL myocytes by immunolabeling with an anti–β-tubulin antibody (red) revealed a fine network spread over the entire cell surrounding myofibrils (blue), with occasional formation of loop-type structures (Figure 2A). After COL treatment (1 μmol/L, 60

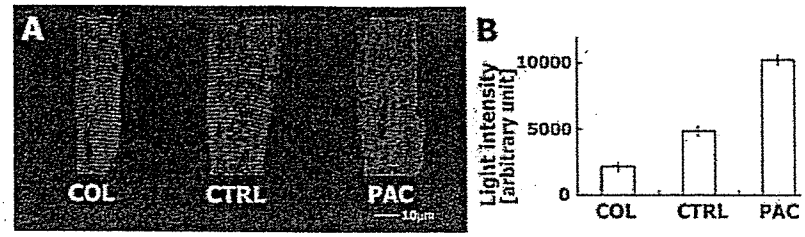

Figure 2. Alterations of microtubule polymerization. A, Immunolabeling of CTRL, COL-treated, and PAC-treated cells with an anti-β-tubulin antibody (red) and actin stain (blue) by rhodamine phalloidin A fine tubulin network spread over the entire cell, with occasional formation of loop-like structures, and perinuclear distribution are observed in CTRL myocytes. After COL treatment, the mesh-like microtubule network almost disappears, whereas PAC treatment significantly increases the number of longitudinal microtubules apposed to the myofibrils. B, These tendencies are confirmed by quantification of the light intensities of the β-tubulin fluorescence (red) in the confocal images normalized to the cell area. COL: n=9; CTRL: n=9; PAC: n=10 cells. P=0.00 for group comparisons by ANOVA.

minutes), the mesh-like microtubule network had almost disappeared, whereas the number of microtubules apposed to myofibrils increased significantly after PAC treatment (10 μmol/L, 3 hour) (Figure 2A). These tendencies were confirmed by quantification of the red-light intensities in confocal images normalized to the cell area (Figure 2B). We also noted that these dynamic changes occurred preferentially in the longitudinal microtubules, consistent with previous immunolabeling light and electron microscopic studies.[25] These drug-induced changes in the microtubule density did not have any effect on the tensile stiffness of the myocytes (Figure 1B).

The transverse stiffness (*Keff*) was 11.6±1.6 nN/μm for CTRL myocytes (n=9). *Keff* tended to change in parallel with the microtubule density (Figure 3B), but the difference did not reach statistical significance (P=0.19 for group comparisons by ANOVA).

We also evaluated the shear stiffness (shear stress/shear strain) in 2 directions, ie, the longitudinal and transverse planes, using a novel technique involving a small glass plate coupled with a carbon fiber (Figure 4A and 4B). The myocyte was held between the bottom coverglass and a small thin glass plate attached onto the top surface. We applied shear stress by shifting the top glass plate connected to a piezoelectric translator via the carbon fiber. Fluorescent staining with a voltage-sensitive indicator (Di2-ANEPEQ) facilitated visualization of the area in contact with the glass plate, and we confirmed that this contact area did not change appreciably during the shear deformation. We confined our analysis to small deformations (linear range) by evaluating the slope at the origin. The shear stiffness values thus obtained for the longitudinal plane (4.57±0.20 kPa, n=15) was nearly double that for the transverse plane (2.94±0.27 kPa, n=13) in CTRL myocytes at 10% strain (Figure 4C and 4D). As in the case of the tensile stiffness, the shear stiffness in the transverse plane did not change significantly by the drug interventions (Figure 4D). However, in the longitudinal plane, hyperpolymerization induced by PAC treatment caused increased the shear stiffness by approximately 2-fold, whereas COL treatment decreased the value by approximately 50% (Figure 4C).

In some myocytes, we evaluated the contribution of cross-bridge formation by repeating these measurements in the calcium-free (Ca 0 mmol/L, EGTA 0.4 mmol/L) solution with 20 mmol/L of butane-dione monoxime (BDM). Inhibition of cross-bridge formation decreased the tensile stiffness

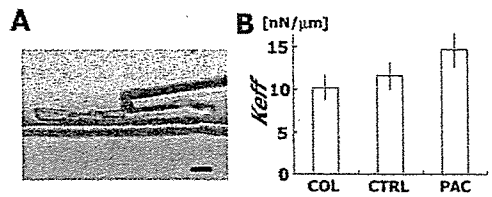

Figure 3. Transverse stiffness. A, Transverse stiffness was evaluated by the indentation test. The cell surface was indented transversely using a small microsphere attached to the carbon fiber. Scale bar=10 μm. B, The transverse stiffness was defined as the effective stiffness (*Keff*) by evaluating the slope of the force-indentation curve at the origin (11.6±1.6 nN/μm for CTRL myocytes, n=9). The transverse stiffness tends to change with the microtubule density after treatment with COL (10.2±1.5 nN/μm, n=10) or PAC (14.7±2.0 nN/μm, n=8), but the differences did not reach statistical significance (P=0.19 for group comparisons by ANOVA).

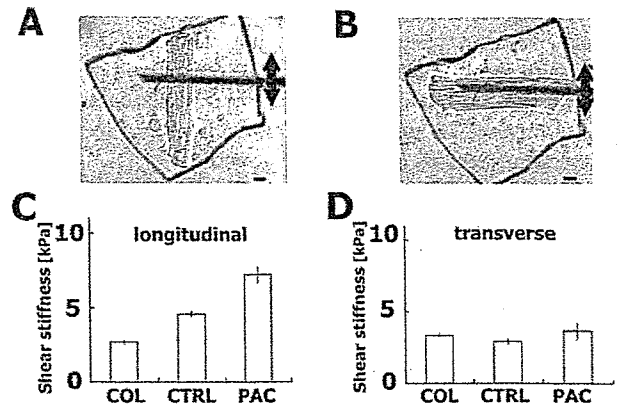

Figure 4. Shear stiffness. A and B, Shear stiffness was evaluated by applying shear stress in both the longitudinal (A) and transverse (B) planes while holding a myocyte between horizontally arranged glass plates. The shear stress was applied by shifting the top glass plate connected to a piezoelectric translator via the carbon fiber. Scale bars=10 μm. C, The shear stiffness (shear stress/shear strain) in longitudinal planes. Shear stiffness of the CTRL myocytes (4.57±0.20 kPa, n=15) increased after treatment with PAC (7.21±0.56 kPa, n=16) and decreased after treatment with COL (2.70±0.14 kPa, n=16) in the long-axis (fiber) direction (P=0.00 by ANOVA). D, The shear stiffness in transverse planes remains unchanged by the drug interventions (CTRL: 2.94±0.27 kPa, n=12; COL: 3.37±0.21 kPa, n=15; PAC: 3.66±0.25 kPa, n=15) (P=0.13 by ANOVA).

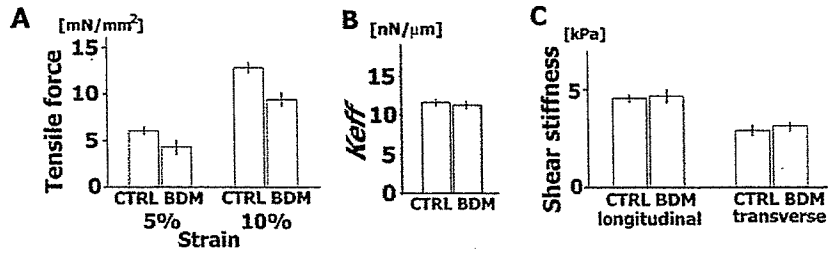

Figure 5. The contribution of cross-bridge formation to tensile stiffness, shear stiffness, and transverse stiffness. A, Inhibition of cross-bridge formation with free extracellular calcium concentration (Ca 0 mmol/L, EGTA 0.4 mmol/L) and 20 mmol/L BDM. BDM decreased the tensile stiffness by 29% at 5% strain and 27% at 10% strain compared with 1.1 mmol/L extracellular calcium (CTRL) (CTRL: 6.02±0.80 mN/mm² at 5% strain and 12.8±0.73 mN/mm² at 10% strain, n=8; BDM: 4.26±0.39 mN/mm² at 5% strain and 9.36±0.60 mN/mm² at 10% strain, n=15) (P=0.04 at 5% strain; P=0.00 at 10%). B, Transverse stiffness was not altered by BDM treatment (20 mmol/L) at the extracellular calcium of 1.1 mmol/L (CTRL: 11.6±0.42 nN/μm, n=12; BDM: 11.2±0.51 nN/μm, n=10; P=0.32). C, Shear stiffness in longitudinal and transverse planes did not change by free extracellular calcium and BDM treatment. (Longitudinal shear stiffness: CTRL, 4.57±0.20, n=15; BDM: 4.69±0.33, n=9; P=0.37.) (Transverse shear stiffness: CTRL, 2.94±0.27 kPa, n=12; BDM: 3.13±0.23 kPa, n=6; P=0.29.)

by 27% at 10% strain (Figure 5A). On the other hand, neither transverse stiffness (Figure 5B) nor shear stiffness in both longitudinal and transverse planes was altered by cross-bridge inhibition (Figure 5C).

Because a previous study showed the effect of microtubules proliferation on the viscosity of the myocardial tissue in response to the tensile deformation,[12] we also evaluated the viscous properties of cardiomyocyte by applying sinusoidal strain of varying frequencies. The elastic (storage) and viscous (loss) components of the stress/strain modulus were estimated using Fourier transform at the frequency between 1 and 10 Hz (corresponding to the strain rate of 0.1 to 1 sec^{-1}) (Figure 6A and 6B). Whereas the elastic moduli did not change appreciably over the examined frequency range, the viscous moduli were dependent on the strain rate. Neither COL nor Taxol treatment altered the relation between the elastic modulus and strain rate, but the PAC treatment increased the slope of the relation between the tensile strain rate and the viscous modulus significantly (COL: 9.4±0.5 mN/mm² per second; CTRL: 11.0±0.8 mN/mm² per second; PAC: 14.8±1.1 mN/mm² per second; n=6 for each, P<0.05 PAC versus COL and CTRL) (Figure 6B). All of these results were consistent with the previous report.[12]

In the case of shear in the longitudinal plane, elastic moduli were also independent of the frequency (Figure 6C), but the average value over the tested range (1.0 to 10 Hz corresponding to the shear rate of 0.5 to 5/sec) differed among the 3 groups (COL: 3.4±0.3 kPa; CTRL: 4.8±0.4 kPa; PAC: 8.4±0.6 kPa; n=6 for each, P<0.05 for group comparisons by ANOVA). Similar to the tensile stiffness measurement, the viscous moduli were dependent on the shear rate (Figure 5D), and the slope of the relation was significantly greater in PAC-treated myocytes (COL: 0.46±0.01 kPa per second; CTRL: 0.46±0.02 kPa per second; PAC: 0.53±0.013 kPa per second; n=6 for each, P<0.05 PAC versus COL and CTRL).

To study the roles of microtubules in pathological conditions, measurements were performed on myocytes from cardiomyopathic (CMP) hamster (Bio-TO2 strain), a well-known hereditary animal model of congestive heart failure[26,27] using Syrian hamsters as CTRL. The CMP myocytes showed increased level of microtubules proliferation, which was normalized after COL treatment (Figure 7A). Tensile stiffness at 10% strain did not differ between the 2 groups (Figure 7B), but longitudinal shear stiffness was increased in CMP. Furthermore, this increase in shear stiffness was normalized by COL treatment (Figure 7C).

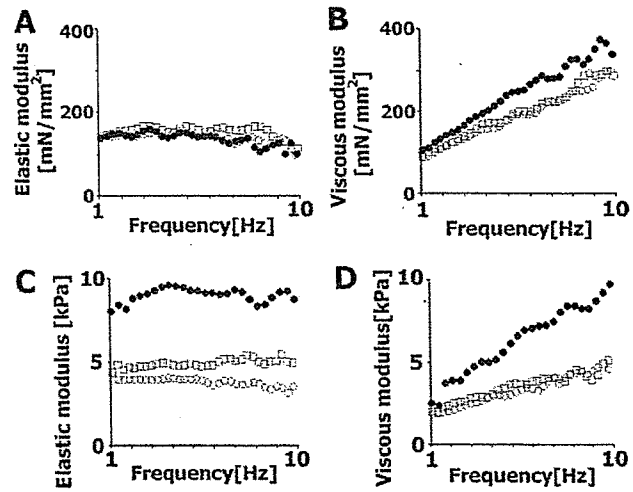

Figure 6. The elastic and viscous modulus. A, The representative data of elastic modulus at 5% tensile strain applied at the frequency between 1 and 10 Hz (COL, open circles; CTRL, open boxes; PAC, closed circles). The elastic moduli averaged over the frequency between 1 and 10 Hz were not different among the 3 groups (COL: 136.3±10.3 mN/mm²; CTRL: 151.2±16.6 mN/mm²; PAC: 141.8±16.4 mN/mm²; n=6 cells for each; not significant). B, The viscous modulus at 5% tensile strain, which was dependent on the strain rate. The slope of the relation between the frequency and the viscous modulus was significantly increased by PAC treatment (COL: 9.4±0.5 mN/mm² per second; CTRL: 11.0±0.8 mN/mm² per second; PAC: 14.8±1.1 mN/mm² per second; n=6 for each; P<0.05 PAC vs COL and CTRL). C, The elastic modulus at 10% shear strain in the longitudinal plane. The elastic moduli were independent of the frequency, but the average value over the tested range (1.0 to 10 Hz) differed among the 3 groups (COL: 3.4±0.3 kPa; CTRL: 4.8±0.4 kPa; PAC: 8.4±0.6 kPa; P<0.05 for group comparisons by ANOVA). D, The viscous modulus at 10% shear strain in the longitudinal plane. Similar to the tensile stiffness measurement, the viscous moduli were dependent on the frequency, and the slope of the relation was significantly greater in PAC treated myocytes (COL: 0.46±0.01 kPa/sec; CTRL: 0.46±0.02 kPa/sec; PAC: 0.53±0.013 kPa/sec; n=6 for each; P<0.05 PAC vs COL and CTRL).

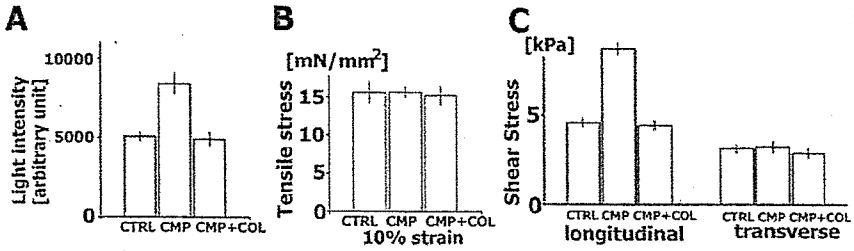

Figure 7. Cell stiffness under pathological condition. A, Proliferation level of microtubules in CMP hamster was elevated compared with the control hamsters (CTRL) but normalized after COL treatment (CMP-COL). The proliferation level was quantified as the light intensities of the anti-tubulin fluorescence in the confocal images normalized to the cell area. (CTRL: n=9; CMP: n=8; CMP-COL: n=10; P=0.00 for group comparisons by ANOVA.) B, Tensile stiffness at 10% strain was not significantly different among 3 groups. (CTRL: 15.6±1.43 mN/mm^2, n=11; CMP: 15.6±0.72 mN/mm^2, n=11; CMP-COL: 15.2±1.28 mN/mm^2, n=10; P=0.96 for group comparisons by ANOVA.) C, Shear stiffness in longitudinal plane was increased in CMP, and normalized by COL treatment. (Longitudinal: CTRL, 4.6±0.43 kPa, n=12; CMP, 8.8±0.67 kPa, n=11; CMP-COL, 4.5±0.39 kPa, n=11; P=0.00 for group comparisons by ANOVA.) (Transverse: CTRL, 3.1±0.21 kPa, n=12; CMP, 3.2±0.31 kPa, n=11; CMP-COL, 2.9±0.26 kPa, n=10; P=0.66 for group comparisons by ANOVA.) Shear stiffness in the transverse plane did not differ among the 3 groups.

Discussion

In the present study, we measured cellular stiffness as well as stiffness against shear deformation in both the longitudinal and transverse planes. From all of these measurements, we found that changes in the microtubule density induced by drug interventions had marked influences on the shear stiffness in the longitudinal plane. In animal model of heart failure, we also demonstrated that the elevated level of microtubule proliferation in pathological condition was associated with an increase in shear stiffness in longitudinal plane, which was normalized by COL treatment.

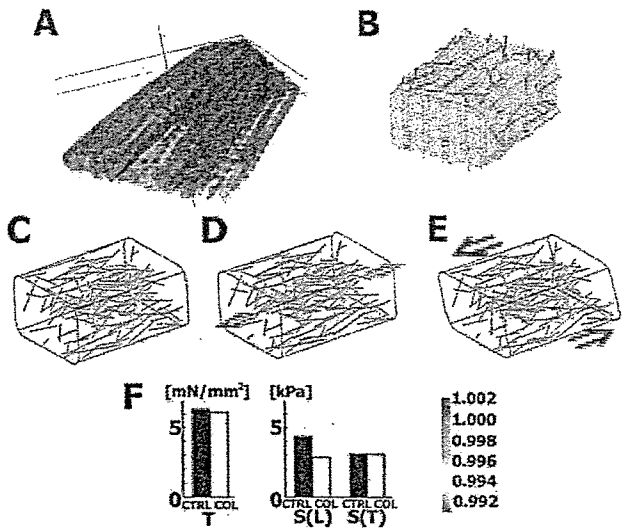

Figure 8. Finite element model of cardiomyocytes. A, Three-dimensional image of cytoskeleton structures. Microtubules were stained by anti-β-tubulin antibody (red) and actin stained by rhodamine phalloidin (blue). The obtained images using confocal microscopy with 0.2-μm thick slices were reconstructed using Micro-AVS software (KGT Inc, Tokyo Japan). B, Schematic representation of the model. Myofibrils (light blue boxes) are interconnected transversely by desmin intermediate filaments (thin red lines). A cytoskeletal network composed of microtubules (thick red rods) and actin filaments (green lines) surrounds the myofibrils. C, Microtubules under control (no-load) conditions are in a compressed state (see color-coding scale, bottom right). D, Microtubules during tensile deformation show no change in the strain-state. E, Some of the microtubules are highly compressed during shear deformation. F, Calculated moduli under 5% tensile (T), 10% longitudinal shear (S(L)), and 10% transverse shear (S(T)) deformation. Black bars indicate control condition; white bars, reduced number of microtubules mimicking COL treatment.

Because microtubules have been implicated in many pathological conditions of the heart, such as cardiac hypertrophy, heart failure, and ischemia,[5,6,28] many researchers have studied their roles in determining the mechanical properties.[11–13,29,30] These studies by applying either stretch or anisoosmotic stress to the myocyte or muscle preparations found no significant change in the passive stiffness of the myocardium[11,12,29,30] but only found an effect on viscosity of the microtubule proliferation. Our measurement using carbon fiber technique confirmed these findings. Quantitative comparison of the viscosity with previous studies is difficult because various indices of viscosity have been used.[12,13] However, in a similar study applying cyclic stretch to the rat papillary muscle,[12] Yamamoto et al reported approximately 1.7 fold increase (estimated from their Figure 7) in the slope of the relation between viscous constant (the area of the hysteresis loop) and the strain rate by PAC treatment. The increase in slope identified in this study (≈1.35) is a little smaller, but the use of different index of viscosity may account for this discrepancy.

Although the effect on the tensile stiffness has not yet been definitely identified, a few studies have suggested the mechanical role of microtubules against shear strain. Tagawa et al,[13] using magnetic twisting cytometry, showed a 100% increase in the stiffness and a 300% increase in the viscosity after microtubule proliferation induced by pressure overload hypertrophy. Recently, Lammerding et al[31] measured local cell stiffness and reported anisotropy in the material properties of adult mouse cardiomyocytes. Their index of local stiffness differed by a factor of 2 between the longitudinal and transverse directions. We also found that, at the baseline, the cellular shear stiffness was anisotropic in nature (also differed by factor of 2), probably reflecting the preferential distribution of the microtubule density in the longitudinal direction.[25] Although the data in these studies[13,31] were obtained by applying rotational shear locally using magnetic twisting cytometry, thus not translated into cellular stiffness measured in this study in a straightforward manner, they can be taken to support the present finding,

The change in cross-bridge state induced by BDM did not affect the shear stiffness. This may be a surprising result if the shear stiffness of the intact myocytes measured in this study directly reflects the property of myofibril. However, as Palmer and Ross have shown in isolated rat cardiomyocytes,[32] the lateral coupling between domains of sarcomeres (myofibril) is loose, and these domains slip in response to externally applied force as if they were solid bodies connected by strings. Therefore, we consider that the shear stiffness measured in the intact myocytes mainly reflects the property of cytoskeleton connecting the myofibrils. Similarly, our index of lateral stiffness derived from the initial phase of contact might not probe the small BDM-induced change in myofibrillar stiffness of the resting myocyte.

Why do microtubules modulate only the stiffness against shear strain without changing the tensile stiffness? Gittes et al[23] measured the flexural rigidity of microtubules and actin filaments to find that the rigidity of microtubules is 3 orders of magnitude greater than that of actin filament. Because the estimated tensile stiffness of a single microtubule was much greater than that of the longitudinal stiffness of the cell, they concluded that, to accommodate strain, microtubules cannot be continuous throughout the length of the cell and that sliding must occur between the filaments. Similar reasoning can be applied to the cardiomyocyte in which microtubule structure has no effect on the tensile stiffness but does affect the viscosity. On the other hand, to modulate the stiffness against shear applied either locally[13] or globally (in the present study), microtubule cytoskeleton must be linked, at least weakly, and anchored to the sarcolemma. We considered that crosslinking with other compliant cytoskeletal structure, eg, actin filament, microtubules can give such mechanical properties to the cardiomyocytes. That is, tensile strain is absorbed by the compliant actin network and the microtubules serve as beams to resist compression when shear stress was applied to the myocytes. The basic idea was similar to the cellular tensegrity model, in which compression-resistant elements (microtubules) support the cell against compression generated by the surrounding tensed cable network to form a structure for mechanotransduction.[1,33]

We developed a simulation model to evaluate this hypothesis. We used the finite element method to model myofilaments, desmin intermediate filaments, cytoskeletal actin filaments, and microtubules as distinct structures with their respective material properties reported in the literature (supplemental Table). Because the constitutive equation of the myofibril is not available currently, we modified and used the constitutive equation of the myocardial tissue proposed by Humphrey et al.[24] Titin, the major determinant of the passive tensile stiffness of cardiac myocyte at shorter sarcomere length,[29] was not modeled as a distinct element, but included in the myofibril. In addition, the following assumptions were made: (1) actin only bears tension and cannot resist compression; (2) microtubules are elastic and preferentially orientated in the longitudinal direction; (3) actin filaments and microtubules are connected to form the cytoskeleton and are anchored to the sarcolemma (outermost elements) in a discrete fashion; and (4) myofilaments are interconnected transversely by desmin intermediate filaments at the Z-line (Figure 8A and 8B). Because we applied a prestretch (1%) to the actin filaments, all the microtubules were in a compressed state under the control condition (coded in blue to green in Figure 8C). Next, we simulated the effects of tensile stress and shear stress using this model. When we applied a stretch (5%) to the cell, the microtubules became rearranged, but no change in the strain status of the microtubules was observed (Figure 8D). On the other hand, application of a shear (10%) induced high compression of some of the microtubules (green to red in Figure 6E). In accordance with the experimental results, in response to a 70% reduction in the number of microtubules (181 to 52), tensile stiffness (T) and shear stiffness in the transverse plane (S(T)) did not change appreciably, whereas the shear stiffness in the longitudinal plane (S(L)) clearly decreased (Figure 6F). Furthermore, we repeated the calculations under different conditions. (1) To examine whether prestress affect these parameters, we repeated the calculation under the condition of zero prestress. (2) Young's modulus of microtubule was raised to 1.2 GPa corresponding to a persistence length of 5200 μm.[23] The changes in the final result were modest in both cases (shown in the online data supplement).

Shear deformation of the cardiac tissue has seldom attracted the interest of researchers, probably because the muscle has been regarded as a linear force generator from the conventional physiological point of view. In reality, however, each cardiomyocyte being stretched and contracted in the complex force field of the ventricular wall undergoes significant shear deformation. Omens et al measured the 3D strain in the isolated arrested canine left ventricle and found that the shear strain reached 0.05 to 0.1 at the endocardium when a 15 mm Hg of intraventricular pressure was applied.[34] Dokos et al[35] measured the shear properties of passive myocardial tissue to find highly anisotropic nature of myocardium reflecting the alignment of myocytes as well as their laminar structure. Also in beating human left ventricle, release of shear deformation has been demonstrated to play a critical role in relaxation.[36] Furthermore, anisotropy in the shear stiffness has also been suggested to play an important role in cardiac function.[37] The present data clearly showed the importance of microtubules in determining such mechanical properties and could establish a link between the constitutive properties of each myocyte and the whole ventricle. In addition, shear stress may also serve to transmit mechanical signals to the nucleus via the microtubule network during the development of cardiac hypertrophy.

Acknowledgments

This study was supported by The Vehicle Racing Commemorative Foundation (to S.S.), The Nakatani Electronic Measuring Technology Association of Japan (to S.S.), and Core Research for Evolutional Science and Technology of the Japan Science and Technology Agency (to T.H. and J.-i.O.). We thank C. Miyazawa for excellent technical assistance.

References

1. Ingber DE. Tensegrity: the architectural basis of cellular mechanotransduction. *Ann Rev Physiol.* 1997;59:575–599.
2. Goode BL, Drubin DG, Barnes G. Functional cooperation between the microtubule and actin cytoskeletons. *Curr Opin Cell Biol.* 2000;12:63–71.

3. Rogers SL, Gelfand VI. Membrane trafficking, organelle transport, and the cytoskeleton. *Curr Opin Cell Biol.* 2000;12:57–62.
4. Samuel J-L, Schwartz K, Lompre A-M, Delcayré C, Marotte F, Swynghedauw B, Rappaport L. Immunological quantitation and localization of tubulin in adult rat heart isolated myocytes. *Eur J Cell Biol.* 1983;31:99–106.
5. Rappaport L, Samuel JL, Bertier B, Bugaisky L, Marotte F, Mercadier A, Schwartz K. Isomyosins, microtubules and desmin during the onset of cardiac hypertrophy in the rat. *Eur Heart J.* 1984;5(Suppl F):243–250.
6. Hein S, Kostin S, Heling A, Maeno Y, Schaper J. The role of the cytoskeleton in heart failure. *Cardiovasc Res.* 2000;45:273–278.
7. Tsutsui H, Ishihara K, Cooper G IV. Cytoskeletal role in the contractile dysfunction of hypertrophied myocardium. *Science.* 1993;260:682–687.
8. Ishibashi Y, Tsutsui H, Yamamoto S, Takahashi M, Imanaka-Yoshida K, Yoshida T, Urabe Y, Sugimachi M, Takeshita A. Role of microtubules in myocyte contractile dysfunction during cardiac hypertrophy in the rat. *Am J Physiol.* 1996;271:H1978–H1987.
9. Cicogna AC, Robinson KG, Conrad CH, Singh K, Squire R, Okoshi MP, Bing OH. Direct effects of colchicine on myocardial function: studies in hypertrophied and failing spontaneously hypertensive rats. *Hypertension.* 1999;33:60–65.
10. de Tombe PP. Altered contractile function in heart failure. *Cardiovasc Res.* 1998;37:367–380.
11. Kato S, Koide M, Cooper G IV, Zile MR. Effects of pressure- or volume-overload hypertrophy on passive stiffness in isolated adult cardiac muscle cells. *Am J Physiol.* 1996;271:2575–2583.
12. Yamamoto S, Tsutsui H, Takahashi M, Ishibashi Y, Tagawa H, Imanaka-Yoshida K, Saeki Y, Takeshita A. Role of microtubules in the viscoelastic properties of isolated cardiac muscle. *J Mol Cell Cardiol.* 1998;30: 1841–1853.
13. Tagawa H, Wang N, Narishige T, Ingber DE, Zile MR, Cooper G IV. Cytoskeletal mechanics in pressure-overload cardiac hypertrophy. *Circ Res.* 1997;80:281–289.
14. Nishimura S, Yasuda S-I, Katoh M, Yamada KP, Yamashita H, Saeki Y, Sunagawa K, Nagai R, Hisada T, Sugiura S. Single cell mechanics of rat cardiomyocytes under isometric, unloaded, and physiologically loaded conditions. *Am J Physiol.* 2004;287:H196–H202.
15. Yasuda S-I, Sugiura S, Kobayakawa N, Fujita H, Yamashita H, Katoh K, SaekI Y, Kaneko H, Suda Y, Nagai R, Sugi H. A novel method to study contraction characteristics of a single cardiac myocyte using carbon fibers. *Am J Physiol.* 2001;281:H1442–H1446.
16. Nyland LR, Maughan DW. Morphology and transverse stiffness of *Drosophila* myofibrils measured by atomic force microscopy. *Biophys J.* 2000;78:1490–1497.
17. Kojima H, Ishijima A, Yanagida T. Direct measurement of stiffness of single actin filaments with and without tropomyosin by *in vitro* nanomanipulation. *Proc Natl Acad Sci U S A.* 1994;91:12962–12966.
18. Kis A, Kasas S, Babic B, Kulik AJ, Benoit W, Briggs GAD, Schonenberger C. Nanomechanics of microtubules. *Phys Rev Lett.* 2002;89:248101.
19. Bar H, Strelkov SV, Sjoberg G, Aebi U, Herrmann H. The biology of desmin filaments: how do mutations affect their structure, assembly, and organization? *J Struct Biol.* 2004;148:137–152.
20. Anderson J, Li F, Goubel F. Models of skeletal muscle to explain the increase in passive stiffness in desmin knockout muscle. *J Biomech.* 2002;35:1315–1324.
21. Kurachi M, Hoshi M, Tashiro H. Buckling of a single microtubule by optical trapping forces: direct measurement of microtubule rigidity. *Cell Motil Cytoskeleton.* 1995;30:221–228.
22. Venier P, Maggs A, Carlier M, Pantaloni D. Analysis of microtubule rigidity using hydrodynamic flow and thermal fluctuations. *J Biol Chem.* 1994;269:13353–13360.
23. Gittes F, Mickey B, Nettleton J, Howard J. Flexural rigidity of microtubules and actin filaments measured from thermal fluctuations in shape. *J Cell Biol.* 1993;120:923–934.
24. Humphrey JD, Strumpf RK, Yin FCP. Determination of a constitutive relation for passive myocardium. I. A new function. *J Biomech Eng.* 1990;112:333–339.
25. Watkins SC, Samuel JL, Marotte F, Bertier-Savalle B, Rappaport L. Microtubules and desmin filaments during onset of heart hypertrophy in rat: a double immunoelectron microscope study. *Circ Res.* 1987;60: 327–336.
26. Nishimura S, Yamashita H, Katoh M, Yamada KP, Sunagawa K, Saeki Y, Ohnuki Y, Nagai R, Sugiura S. Contractile dysfunction of cardiomyopathic hamster myocytes is pronounced under high load conditions. *J Mol Cell Cardiol.* 2005;39:231–239.
27. Kruger C, Erdmann E, Nabauer M, Beuckelmann DJ. Intracellular calcium handling in isolated ventricular myocytes from cardiomyopathic hamsters (strain BIO 14.6) with congestive heart failure. *Cell Calcium.* 1994;16:500–508.
28. Sato H, Hori M, Kitakaze M, Iwai K, Takashima S, Kurihara H, Inoue M, Kamada T. Reperfusion after brief ischemia disrupts the microtubule network in canine hearts. *Circ Res.* 1993;72:361–375.
29. Granzier HL, Irving TC. Passive tension in cardiac muscle: contribution of collagen, titin, microtubules, and intermediate filaments. *Biophys J.* 1995;68:1027–1044.
30. Zile MR, Richardson K, Cowels MK, Buckley JM, Koide M, Cowels BA, Gharpuray V, Cooper G IV. Constitutive properties of adult mammalian cardiac muscle cells. *Circulation.* 1998;98:567–579.
31. Lammerding HH, Huang H, So PT, Kamm RD, Lee RT Quantitative measurement of active and passive mechanical properties of adult cardiac myocytes. *IEEE Eng Med Biol Mag.* 2003:124–127.
32. Palmer RE, Roos KP. Extent of radial sarcomere coupling revealed in passively stretched cardiac myocytes. *Cell Motil Cytoskeleton.* 1997;37: 378–388.
33. Wang N, Butler JP, Ingber DE. Mechanotransductions across the cell surface and through the cytoskeleton. *Science.* 1993;260:1124–1127.
34. Omens JH, May KD, McCulloch AD. Transmural distribution of three-dimensional strain in the isolated arrested canine left ventricle. *Am J Physiol.* 1991;261:H918–H928.
35. Dokos S, Smaill BH, Young AA, LeGrice IJ. Shear properties of passive ventricular myocardium. *Am J Physiol Heart Circ Physiol.* 2002;283: H2650–H2659.
36. Rosen BZ, Gerber BL, Edvardsen T, Castillo E, Amado LC, Nasir K, Kraitchman DL, Osman NF, Bluemke DA, Lima JAC. Late systolic onset of regional LV relaxation demonstrated in three-dimensional space by MRI tissue tagging. *Am J Physiol.* 2004;287:H1740–H1746.
37. LeGrice IL, Takayama Y, Covell JW. Tranverse shear along myocardial cleavage planes provides a mechanism for normal systolic wall thickening. *Circ Res.* 1995;77:182–193.